ELSEVIER

Chemical Engineering Journal 115 (2005) 23–43

Chemical Engineering Journal

www.elsevier.com/locate/cej

Linoleic acid isomerization on Ru/Al_2O_3 catalyst 2. Elementary step mechanism and data fitting

Andreas Bernas, Dmitry Yu. Murzin *

Laboratory of Industrial Chemistry, Process Chemistry Centre, Åbo Akademi University, Biskopsgatan 8, FIN-20500 Åbo/Turku, Finland

Received 8 March 2005; received in revised form 19 August 2005; accepted 26 August 2005

Abstract

The selective double bond isomerization reaction of linoleic acid to *cis*-9,*trans*-11-conjugated linoleic acid and *trans*-10,*cis*-12-conjugated linoleic acid on commercial H_2-preactivated Ru/Al_2O_3 catalyst studied at 135–165 °C under kinetic control in a slurry reactor under atmospheric pressure in *n*-decane solution using the linoleic acid-to-surface ruthenium molar ratios 2.5, 5, and 10, was investigated by mathematical modeling. Over such catalyst and at the conditions used, the reaction scheme involves competitive isomerization of linoleic acid to conjugated linoleic acid isomers as well as hydrogenation of linoleic acid to oleic acid. These competing steps are through a complex relation strongly affected by chemisorbed hydrogen on the Ru surface. The concentrations of chemisorbed hydrogen and adsorbed key intermediates on the ruthenium surface influenced the catalytic activity and the selectivities toward isomerization and hydrogenation products through a complex relation. The isomerization rate was enhanced by catalyst preactivation under hydrogen, but increased hydrogen coverage on the Ru surface also restrained the isomerization selectivity. A reaction network and mechanism were advanced. Mechanistic models were developed from proposed elementary stage mechanism and corresponding kinetic equations were derived. Data fitting allowed discrimination between rival mechanistic models, more specifically the influence of hydrogen on the isomerization kinetics.

Keywords: Conjugated linoleic acid (CLA); Ru/Al_2O_3 catalyst; H_2-preactivation; Kinetic modeling; Double bond migration; Isomerization; Hydrogenation

1. Introduction

In the selective double bond isomerization reaction of linoleic acid to *cis*-9,*trans*-11-conjugated linoleic acid and *trans*-10,*cis*-12-conjugated linoleic acid (CLA) isomers over aluminium oxide supported ruthenium catalyst, one of linoleic acids two double bond migrates to form a conjugated system [1–6]. This is the second paper in the series aiming to investigate the kinetics of Ru/Al_2O_3 catalyzed linoleic acid isomerization at different conditions and to present a kinetic model, which is consistent with mechanistic data and observed kinetic regularities.

2. Catalytic surface reactions

Over supported metal catalysts [1–6], the reaction network involves six steps: (1) double bond migration of linoleic acid to conjugated linoleic acid, (2) positional and geometric isomerization of conjugated linoleic acid, (3) double bond hydrogenation of linoleic acid to mono-enoic acids, (4) double bond hydrogenation of conjugated linoleic acid to mono-enoic acids, (5) positional and geometric isomerization of mono-enoic acids, and (6) double bond hydrogenation of mono-enoic acids to stearic acid. In the following discussion, the term isomerization refers to double bond migration yielding a conjugated system. The sum of the overall isomerization selectivity and the hydrogenation selectivity is equal to unity.

A detailed description of the characterization of the Ru/Al_2O_3 catalyst by nitrogen adsorption, X-ray photoelectron spectroscopy, scanning electron microscopy-energy dispersive X-ray analysis, and temperature programmed desorption of hydrogen techniques as well as a detailed description of the linoleic acid

* Corresponding author. Tel.: +358 2 215 4985; fax: +358 2 215 4479.
E-mail addresses: abernas@abo.fi (A. Bernas), dmurzin@abo.fi (D.Yu. Murzin).

1385-8947/$ – see front matter © 2005 Elsevier B.V. All rights reserved.
doi:10.1016/j.cej.2005.08.013

Nomenclature

a	activity
a_0	initial activity
A	linoleic acid
B	*cis*-9,*trans*-11-CLA
c	concentration
c	model constants
C	*trans*-10,*cis*-12-CLA
C_{18}	18 carbon atom fatty acids
d	order of deactivation
D	*trans*-9,*trans*-11-CLA
E	*cis*-9,*cis*-11-CLA
E_a	activation energy
E_d	activation energy or temperature dependency of deactivation
H	hydrogen
I	number of intermediates
k	kinetic constant
k_d	deactivation constant
k_{d0}	frequency factor of deactivation
k^0	pre-exponential/frequency factor
K	equilibrium factor
L	oleic acid
m	catalyst mass
$N(i)$	independent basic route i
N	mole fraction
N	number of basic routes
p	pressure
Q	conversion independent constant
r	consumption/generation rate
r_{iso}	overall linoleic acid isomerization rate
r_{hydr}	linoleic acid hydrogenation rate
$-r_A$	rate at which the catalyst converts reactant **A**
$-r_{A0}$	rate of reaction of **A** with a fresh catalyst
R	sum of kinetic constants k_{11}, k_{12}, k_{13}, k_{14}, and k_{15}
R^2	coefficient of determination
R_{gas}	the gas constant
s	state of the system
S	sum of kinetic constants k_4, k_5, k_6, k_7, and k_8
S	number of stages
SRS	sum of residual squares
t	unit time
T	reaction temperature
T_{mean}	mean temperature of the experiments
U	unknown CLA isomer
w	weight matrix for observations
W	number of balance equations
x	design variables
$\overline{y}$	average of data points
y_p,	response variables
Z	vacant surface site for chemisorption of organic molecule
Z′	vacant surface site for chemisorption of hydrogen
Zi	chemisorbed compound i
Z′H	chemisorbed hydrogen
ZI(1)	chemisorbed half-hydrogenated intermediates derived from **A**
ZI(2)	chemisorbed dehydrogenated intermediates derived from **A**

Greek letters

Ξ	chemical equilibrium
θ	estimated parameters
θ_i	fractional surface coverage of chemisorbed compound i
$\theta_{I(1)}$	fractional surface coverage of chemisorbed half-hydrogenated intermediates derived from **A**
$\theta_{I(2)}$	fractional surface coverage of chemisorbed dehydrogenated intermediates derived from **A**
θ_0	fractional surface coverage of vacant sites
θ'_H	fractional surface coverage of chemisorbed hydrogen

isomerization, product analysis procedures and investigation of external and internal mass transfer are given in our previous report [7].

3. Mathematical modeling

3.1. Elementary step mechanism

The double bond migration reaction of linoleic acid to CLA over H_2-preactivated Ru/Al_2O_3 catalyst is thought to occur via the Horiuti–Polanyi mechanism [8] describing hydrogenation and isomerization of olefins. After the initial H_2-preactivation, linoleic acid is chemisorbed by the ruthenium surface. Thereafter, a hydrogen atom derived from a hydrogen-chemisorbed site is added to the chemisorbed acid to give a chemisorbed half-hydrogenated intermediate. If the hydrogen coverage on the catalyst surface is rather low, predominantly hydrogen abstraction by the metal takes place from an adjacent carbon atom, which might lead to a double bond migration depending from which carbon atom hydrogen is abstracted. If, on the other hand, the coverage of hydrogen is high, a second hydrogen atom is mainly added to the chemisorbed half-hydrogenated intermediate to result in a double bond hydrogenation. Free rotation of the half-hydrogenated intermediate, hydrogen abstraction, and desorption of the olefin result in *cis*/*trans*-isomerizations.

If, on the other hand, the first catalytic stage involves C–H bond cleavage, an allylic intermediate is formed on a supported metal atom or on an acidic site. Subsequent hydrogenation at a different carbon atom results in double bond migration [9].

Based on the obtained data, activity and selectivity can be treated separately. For further discussion, let us briefly analyze the reaction network and reaction kinetics. At present optimal conditions, the surface reaction network can be significantly simplified. As proposed in Fig. 1, linoleic acid undergoes isomerization to *cis*-9,*trans*-11-CLA, *trans*-10,*cis*-12-CLA, *trans*-9,*trans*-11-CLA, *cis*-9,*cis*-11-CLA, and an unknown

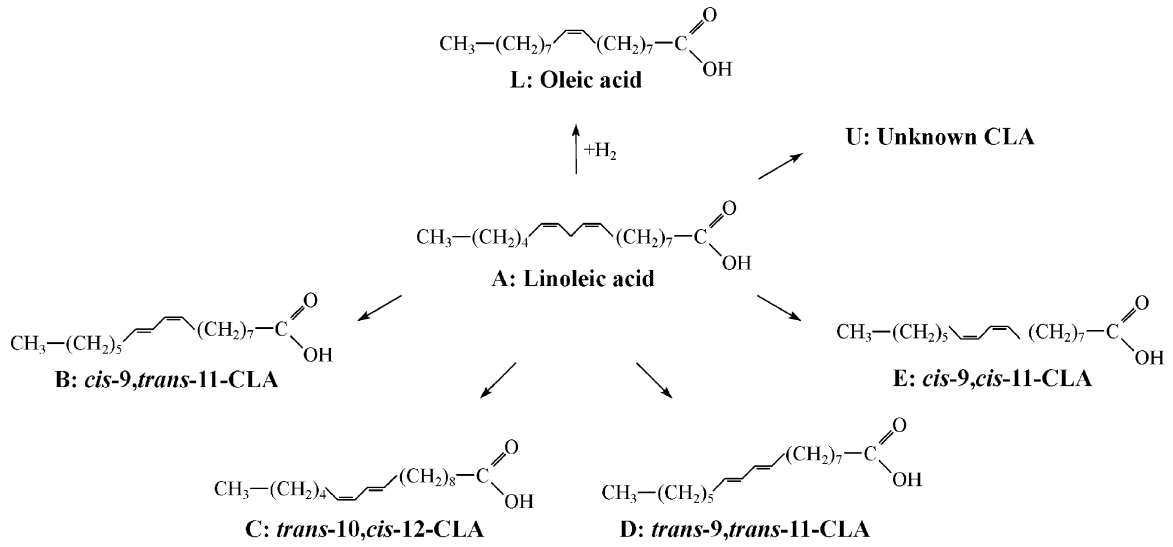

Fig. 1. Main linoleic acid isomerization and hydrogenation network over Ru/Al_2O_3 catalyst.

CLA isomer as well as hydrogenation to oleic acid which is the main mono-unsaturated compound. Linoleic acid, *cis*-9,*trans*-11-CLA, *trans*-10,*cis*-12-CLA, *trans*-9,*trans*-11-CLA, *cis*-9,*cis*-11-CLA, the unknown CLA isomer, and oleic acid are hereafter referred to as **A**, **B**, **C**, **D**, **E**, **U**, and **L**, respectively. Hydrogenation of **L** to stearic acid is neglected since the mole fraction of stearic acid was less than one percent at all reaction temperatures and catalyst masses. Moreover, the hydrogenation reactions of **B**, **C**, **D**, **E**, and **U** to **L** and the positional and geometric isomerization between **B**, **C**, **D**, **E**, and **U** can be neglected because in the present study, no typical consecutive trends of the isomerization kinetics were detected and the selectivity to any compound within the CLA group is rather independent on conversion, as demonstrated in Fig. 2. In fact, in the reaction temperature interval of 135–165 °C and in the catalyst mass interval of 0.2–0.8 g, the ratios between the product concentrations at any reaction time or conversion, and thereby the ratios between the net reaction product generation rates, of any pair of products **B**, **C**, **D**, **E**, and **U**, for example, **C** versus **B**, **D** versus **B**, etc., are constant values, as Fig. 3(a–d) demonstrate. The selectivity to any CLA compound is conversion independent while the selectivity to **L**, on the other hand, increases with the catalyst mass, as shown in Fig. 3(e), since a higher catalyst mass contributes to a larger total amount of hydrogen in the system, which is promoting the double bond hydrogenation step of **A** to **L**.

Consequently, following basic facts were considered in the build-up of the kinetic model:

(1) **A** is the single olefinic acid that undergoes hydrogenation to **L**.
(2) Isomerization and hydrogenation of **A** are two irreversible competing parallel reactions.
(3) The isomerization reactions within the CLA group can be neglected.
(4) There are no non-catalytic isomerization or hydrogenation reactions of **A**.
(5) Double bond migration and double bond hydrogenation take place through the Horiuti–Polanyi mechanism. Moreover, double bond migration takes place through a dehydrogenation pathway.

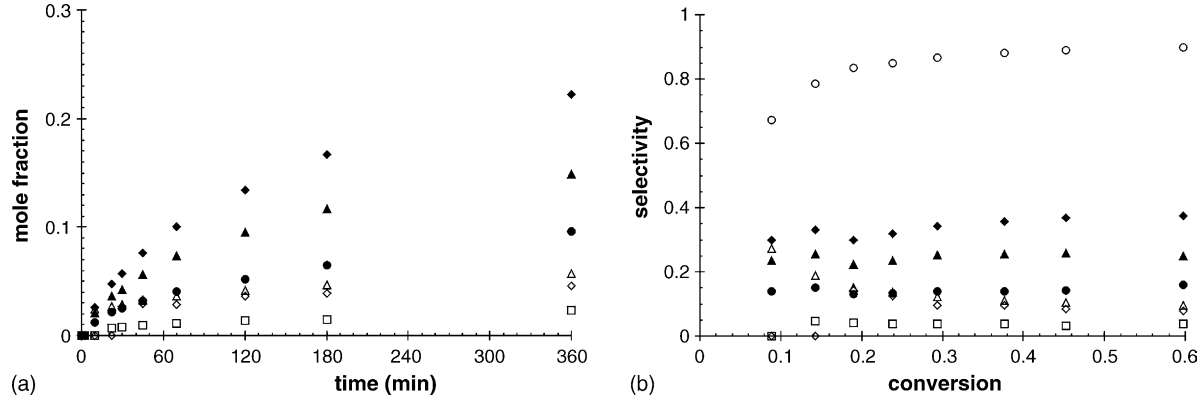

Fig. 2. (a) Kinetics of CLA generation and (b) dependence of selectivity on conversion in linoleic acid isomerization on H_2-preactivated Ru/Al_2O_3 catalyst: (♦) **B**, (▲) **C**, (●) **D**, (□) **E**, (◊) **U**, (△) **L**, (◯) overall isomerization. *Conditions*: raw material, 0.2 g of reagent grade linoleic acid; solvent, 70 ml of *n*-decane; catalyst mass, 0.8 g; catalyst metal loading, 6.2 wt%; catalyst particle diameter interval, 0–63 μm; stirring rate, 800 rpm; reaction temperature, 165 °C; H_2-preactivation temperature, 100 °C; H_2-preactivation time, 1 h; reaction pressure, 1 atm of nitrogen; reaction time, 6 h.

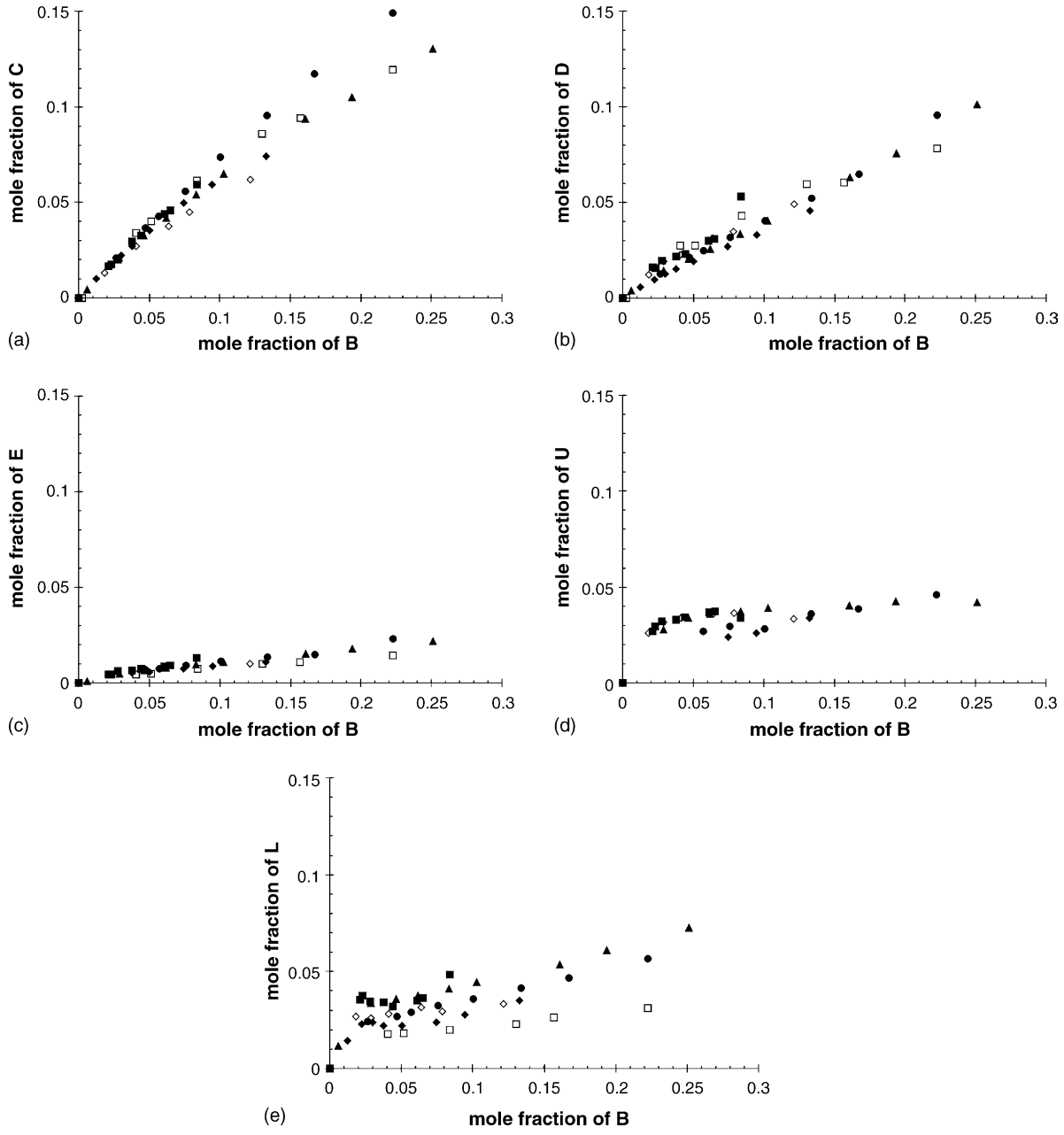

Fig. 3. Compositions of (a) **C** vs. **B**, (b) **D** vs. **B**, (c) **E** vs. **B**, (d) **U** vs. **B**, and (e) **L** vs. **B** in linoleic acid isomerization on H_2-preactivated Ru/Al_2O_3 catalyst at varied levels of reaction temperature and catalyst mass: (■) 135/0.8, (♦) 145/0.8, (▲) 155/0.8, (●) 165/0.8, (□) 165/0.4, (◊) 165/0.2; stirring rate, 800 rpm. Other conditions same as Fig. 2.

(6) Adsorption of hydrogen and adsorption of organic molecules is non-competitive in nature, hence sites for chemisorption of hydrogen and sites for chemisorption of organic molecules are separated.
(7) Adsorption of **A**, CLA, **L**, and *n*-decane is competitive in nature.
(8) **A** is chemisorbed either through one or through both olefinic bonds. One active site, denoted with Z, is used for chemisorption of only one olefinic acid molecule or one intermediate.
(9) The catalytic surface reactions are irreversible while adsorption/desorption steps of **A** and products are at equilibrium.
(10) Diffusion of linoleic acid from the bulk of the solution to the vicinity of the catalyst does not influence the consumption rate of **A**.
(11) The internal effectiveness factor is 1.
(12) Except for hydrogenation of **A** to **L**, no side reactions occur.

The above mechanism can be presented as follows: linoleic acid isomerization on Ru/Al_2O_3 corresponding to the simplified scheme can be described by 11 reaction routes, i.e. sets of stoichiometric numbers of steps, and written as

Elementary steps	Basic routes										
	$N(1)$	$N(2)$	$N(3)$	$N(4)$	$N(5)$	$N(6)$	$N(7)$	$N(8)$	$N(9)$	$N(10)$	$N(11)$
1. $2Z' + H_2 \overset{K_1}{\Xi} 2Z'H$	0	0	0	0	0	1	0	0	0	0	0
2. $Z + \mathbf{A} \overset{K_2}{\Xi} Z\mathbf{A}$	1	1	1	1	1	1	1	1	1	1	1
3. $Z\mathbf{A} + Z'H \xrightarrow{k_3} ZI(1) + Z'$	1	1	1	1	1	1	0	0	0	0	0
4. $ZI(1) + Z' \xrightarrow{k_4} Z\mathbf{B} + Z'H$	1	0	0	0	0	0	0	0	0	0	0
5. $ZI(1) + Z' \xrightarrow{k_5} Z\mathbf{C} + Z'H$	0	1	0	0	0	0	0	0	0	0	0
6. $ZI(1) + Z' \xrightarrow{k_6} Z\mathbf{D} + Z'H$	0	0	1	0	0	0	0	0	0	0	0
7. $ZI(1) + Z' \xrightarrow{k_7} Z\mathbf{E} + Z'H$	0	0	0	1	0	0	0	0	0	0	0
8. $ZI(1) + Z' \xrightarrow{k_8} Z\mathbf{U} + Z'H$	0	0	0	0	1	0	0	0	0	0	0
9. $ZI(1) + Z'H \xrightarrow{k_9} Z\mathbf{L} + Z'$	0	0	0	0	0	1	0	0	0	0	0
10. $Z\mathbf{A} + Z' \xrightarrow{k_{10}} ZI(2) + Z'H$	0	0	0	0	0	0	1	1	1	1	1
11. $ZI(2) + Z'H \xrightarrow{k_{11}} Z\mathbf{B} + Z'$	0	0	0	0	0	0	1	0	0	0	0
12. $ZI(2) + Z'H \xrightarrow{k_{12}} Z\mathbf{C} + Z'$	0	0	0	0	0	0	0	1	0	0	0
13. $ZI(2) + Z'H \xrightarrow{k_{13}} Z\mathbf{D} + Z'$	0	0	0	0	0	0	0	0	1	0	0
14. $ZI(2) + Z'H \xrightarrow{k_{14}} Z\mathbf{E} + Z'$	0	0	0	0	0	0	0	0	0	1	0
15. $ZI(2) + Z'H \xrightarrow{k_{15}} Z\mathbf{U} + Z'$	0	0	0	0	0	0	0	0	0	0	1
16. $Z\mathbf{B} \overset{K_{16}}{\Xi} Z + \mathbf{B}$	1	0	0	0	0	0	1	0	0	0	0
17. $Z\mathbf{C} \overset{K_{17}}{\Xi} Z + \mathbf{C}$	0	1	0	0	0	0	0	1	0	0	0
18. $Z\mathbf{D} \overset{K_{18}}{\Xi} Z + \mathbf{D}$	0	0	1	0	0	0	0	0	1	0	0
19. $Z\mathbf{E} \overset{K_{19}}{\Xi} Z + \mathbf{E}$	0	0	0	1	0	0	0	0	0	1	0
20. $Z\mathbf{U} \overset{K_{20}}{\Xi} Z + \mathbf{U}$	0	0	0	0	1	0	0	0	0	0	1
21. $Z\mathbf{L} \overset{K_{21}}{\Xi} Z + \mathbf{L}$	0	0	0	0	0	1	0	0	0	0	0

Overall reactions—$N(1)$, $N(7)$: $\mathbf{A} \rightarrow \mathbf{B}$; $N(2)$, $N(8)$: $\mathbf{A} \rightarrow \mathbf{C}$; $N(3)$, $N(9)$: $\mathbf{A} \rightarrow \mathbf{D}$; $N(4)$, $N(10)$: $\mathbf{A} \rightarrow \mathbf{E}$; $N(5)$, $N(11)$: $\mathbf{A} \rightarrow \mathbf{U}$; $N(6)$: $\mathbf{A} + H_2 \rightarrow \mathbf{L}$.

In the catalytic stages, symbols Z, Z′, and H denote vacant surface site for chemisorption of organic molecule, vacant surface site for chemisorption of hydrogen, and atomic hydrogen, respectively. Chemisorbed compounds are described by Z**A**, Z**B**, etc. Symbols Ξ, k, and K denote chemical equilibrium, kinetic constants, and equilibrium factor. The two types of adsorbed intermediate species on the catalyst surface are grouped together in symbols ZI(1) and ZI(2), which denote chemisorbed half-hydrogenated intermediates and chemisorbed dehydrogenated intermediates, correspondingly, both descending from **A**.

Elementary reactions are grouped in steps, and chemical equations of stages contain reactants and surface species. On the right hand side of the equations of stages, the stoichiometric numbers (positive, negative, of zero) for the different independent routes ($N(1)$, etc.) of the complex heterogeneous catalytic reaction are given. These numbers must be chosen in a way that the overall equations contain no surface species. The equations describing the overall reaction are obtained by the summation of chemical equations of stages multiplied by the stoichiometric numbers. A set of stoichiometric numbers of stages is defined as a reaction route [10,11]. Routes must be essentially different, and it is impossible to obtain one route through multiplication of another route by a number, although their respective overall equations can be identical. In the case of Ru/Al_2O_3 catalyzed linoleic acid isomerization where overall reaction are irreversible, the number of basic routes, N, is determined by the following equation:

$$N = S + W - I \tag{1}$$

where S is the number of stages, W the number of balance equations, and I is the number of intermediates. Balance equations determine the relationship between adsorbed intermediates. Such equations can correspond to the total coverage equal to unity. It follows from Eq. (1) that there are 21 equations of stages, 12 intermediates, and 2 balance equations as there are two different types of sites, and consequently 11 basic routes.

In the first stage, hydrogen dissociates on the ruthenium surface. Stage 2 and stages 16–21 describe adsorption and desorption of **A** and products. In basic routes $N(1)$–$N(5)$, stage 3 describe hydrogen addition to chemisorbed **A** resulting in chemisorbed half-hydrogenated intermediates ZI(1) while stages 4–8 described hydrogen abstraction from these intermediates giving chemisorbed CLA isomers. Similarly, in basic routes $N(7)$–$N(11)$, stage 10 describes abstraction of a hydrogen atom from chemisorbed **A** to give a chemisorbed dehydrogenated intermediate ZI(2) while stages 11–15 described hydrogen addi-

tion to these intermediates to give chemisorbed CLA isomers. In basic route *N*(6), stage 9 correspond to addition of a hydrogen atom to intermediate ZI(1) resulting in chemisorbed **L** according to the hydrogen addition part of the Horiuti–Polanyi mechanism [8]. Deactivation stages are not depicted in this mechanism.

3.2. Rate equations

It is assumed that the surface of the catalyst is uniform or quasiuniform meaning that rate constants are coverage independent and that organic compounds form an ideal liquid mixture. Speaking in terms of kinetics, the rate equations for each stage can be written as

$$r_3 = k_3\theta_A\theta'_H \quad (2)$$

$$r_4 = k_4\theta_{I(1)}(1-\theta'_H) \quad (3)$$

$$r_5 = k_5\theta_{I(1)}(1-\theta'_H) \quad (4)$$

$$r_6 = k_6\theta_{I(1)}(1-\theta'_H) \quad (5)$$

$$r_7 = k_7\theta_{I(1)}(1-\theta'_H) \quad (6)$$

$$r_8 = k_8\theta_{I(1)}(1-\theta'_H) \quad (7)$$

$$r_9 = k_9\theta_{I(1)}\theta'_H \quad (8)$$

$$r_{10} = k_{10}\theta_A(1-\theta'_H) \quad (9)$$

$$r_{11} = k_{11}\theta_{I(2)}\theta'_H \quad (10)$$

$$r_{12} = k_{12}\theta_{I(2)}\theta'_H \quad (11)$$

$$r_{13} = k_{13}\theta_{I(2)}\theta'_H \quad (12)$$

$$r_{14} = k_{14}\theta_{I(2)}\theta'_H \quad (13)$$

$$r_{15} = k_{15}\theta_{I(2)}\theta'_H \quad (14)$$

where r, k, and θ denote reaction rate, rate constant, and fractional surface coverage, respectively. In Eqs. (3)–(7) and Eq. (9) vacant sites for hydrogen are expressed directly via hydrogen coverage.

The rates for the adsorption–desorption stages are assumed to be high compared to the rate of the complex reaction as a whole. Thus, the equilibrium constants, K, for these stages are given by

$$K_1 = \frac{\theta'^2_H}{(1-\theta'_H)^2 p_{H_2}} \quad (15)$$

$$K_2 = \frac{\theta_A}{\theta_0 c_A} \quad (16)$$

$$K_{16} = \frac{\theta_0 c_B}{\theta_B} \quad (17)$$

$$K_{17} = \frac{\theta_0 c_C}{\theta_C} \quad (18)$$

$$K_{18} = \frac{\theta_0 c_D}{\theta_D} \quad (19)$$

$$K_{19} = \frac{\theta_0 c_E}{\theta_E} \quad (20)$$

$$K_{20} = \frac{\theta_0 c_U}{\theta_U} \quad (21)$$

$$K_{21} = \frac{\theta_0 c_L}{\theta_L} \quad (22)$$

where c denotes concentration of respective species.

The overall linoleic acid isomerization rate, r_{iso}, and the linoleic acid hydrogenation rate, r_{hydr}, can be defined as

$$r_{iso} = r_4 + r_5 + r_6 + r_7 + r_8 + r_{11} + r_{12} + r_{13} + r_{14} + r_{15} \quad (23)$$

and

$$r_{hydr} = r_9 \quad (24)$$

Deriving kinetic equations from the mechanism above, one arrives at the following expression, which relates the overall isomerization selectivity and the selectivity to **L**:

$$\frac{r_{iso}}{r_{hydr}} = \frac{r_4 + r_5 + r_6 + r_7 + r_8 + r_{11} + r_{12} + r_{13} + r_{14} + r_{15}}{r_9} \quad (25)$$

An insertion of Eqs. (3)–(8) and Eqs. (10)–(14) in Eq. (25) gives the expression

$$\frac{r_{iso}}{r_{hydr}} = \frac{R\theta_{I(1)}\left(1-\theta'_H\right) + S\theta_{I(2)}\theta'_H}{k_9\theta_{I(1)}\theta'_H} \quad (26)$$

where

$$R = k_4 + k_5 + k_6 + k_7 + k_8 \quad (27)$$

and

$$S = k_{11} + k_{12} + k_{13} + k_{14} + k_{15} \quad (28)$$

This relation, which describes the ratio of CLA to **L** generation rates, will increase when θ'_H and $\theta_{I(1)}$ decrease and when $\theta_{I(2)}$ increases. Such a connection indicates that a low fractional coverage on the catalyst surface of chemisorbed hydrogen, a low coverage of the chemisorbed half-hydrogenated intermediates, and a high coverage of the chemisorbed dehydrogenated intermediates favors the overall isomerization reaction, as expected. Accordingly, the isomerization selectivity versus conversion dependence is slightly increasing while the hydrogenation selectivity versus conversion dependence, on the other hand, decreases with conversion, as demonstrated in our previous paper [7], since a part of chemisorbed hydrogen on the ruthenium surface is consumed in the hydrogenation step during the course of the reaction. In essence, the availability of hydrogen affects the ratio given in Eq. (26) and the selectivity pattern.

In addition, Eq. (26) explains why the isomerization selectivity is vaguely higher over a non-preactivated metal catalyst with lower surface coverage of hydrogen than that over hydrogen-preactivated catalyst with high hydrogen coverage, a phenomenon that also came visible in our previous paper [7]. This effect is to a larger extent noted at lower reaction temperatures, which in turn gives higher hydrogen coverage on the catalyst surface [4].

It should also be noted that Eq. (26) reveals the fact that the isomerization selectivity decreases with decreased reaction temperature, which increases the value of the parameter θ'_H, as shown earlier ([7]; Table 2, entries 3 and 9–11).

If more of the CLA is generated via the allylic mechanism, where hydrogen abstraction is followed by hydrogen addition, than via the Horiuti–Polanyi mechanism, where hydrogen takes part as an astoichiometric component by hydrogen addition followed by hydrogen abstraction, the overall isomerization selectivity will increase. Most of **A** reacts via intermediate $\theta_{I(1)}$ if the sum R is larger than S and via intermediate $\theta_{I(2)}$ if S is larger than R.

The consumption/generation rates are defined by

$$r_A = -\frac{1}{m}\frac{dc_A}{dt} = r_3 + r_{10} = k_3\theta_A\theta'_H + k_{10}\theta_A(1-\theta'_H) \quad (29)$$

$$r_B = \frac{1}{m}\frac{dc_B}{dt} = r_4 + r_{11} = k_4\theta_{I(1)}(1-\theta'_H) + k_{11}\theta_{I(2)}\theta'_H \quad (30)$$

$$r_C = \frac{1}{m}\frac{dc_C}{dt} = r_5 + r_{12} = k_5\theta_{I(1)}(1-\theta'_H) + k_{12}\theta_{I(2)}\theta'_H \quad (31)$$

$$r_D = \frac{1}{m}\frac{dc_D}{dt} = r_6 + r_{13} = k_6\theta_{I(1)}(1-\theta'_H) + k_{13}\theta_{I(2)}\theta'_H \quad (32)$$

$$r_E = \frac{1}{m}\frac{dc_E}{dt} = r_7 + r_{14} = k_7\theta_{I(1)}(1-\theta'_H) + k_{14}\theta_{I(2)}\theta'_H \quad (33)$$

$$r_U = \frac{1}{m}\frac{dc_U}{dt} = r_8 + r_{15} = k_8\theta_{I(1)}(1-\theta'_H) + k_{15}\theta_{I(2)}\theta'_H \quad (34)$$

$$r_L = \frac{1}{m}\frac{dc_L}{dt} = r_9 = k_9\theta_{I(1)}\theta'_H \quad (35)$$

where m denotes total catalyst mass. Steady state approximations for intermediates $\theta_{I(1)}$ and $\theta_{I(2)}$ give, respectively, the equations

$$r_3 = r_4 + r_5 + r_6 + r_7 + r_8 + r_9 \quad (36)$$

and

$$r_{10} = r_{11} + r_{12} + r_{13} + r_{14} + r_{15} \quad (37)$$

Insertion of Eqs. (2)–(14) in Eq. (36) and in Eq. (37) yields the expressions

$$k_3\theta_A\theta'_H = R\theta_{I(1)}(1-\theta'_H) + k_9\theta_{I(1)}\theta'_H \quad (38)$$

and

$$k_{10}\theta_A(1-\theta'_H) = S\theta_{I(2)}\theta'_H \quad (39)$$

Coverage of intermediate species $\theta_{I(1)}$ can be obtained from Eq. (38)

$$\theta_{I(1)} = \frac{k_3\theta_A\theta'_H}{R(1-\theta'_H) + k_9\theta'_H} \quad (40)$$

Accordingly, coverage of intermediate $\theta_{I(2)}$ is obtained from Eq. (39)

$$\theta_{I(2)} = \frac{k_{10}\theta_A(1-\theta'_H)}{S\theta'_H} \quad (41)$$

Solving Eq. (41) for θ_A

$$\theta_A = \frac{S\theta'_H\theta_{I(2)}}{k_{10}(1-\theta'_H)} \quad (42)$$

and inserting Eq. (42) into Eq. (40) gives a relation $\theta_{I(1)} = f(\theta_{I(2)})$,

$$\theta_{I(1)} = \frac{k_3 S\theta_{I(2)}\theta'^2_H}{k_{10}(1-\theta'_H)\left[R(1-\theta'_H) + k_9\theta'_H\right]} \quad (43)$$

which can be written as

$$\frac{\theta_{I(1)}}{\theta_{I(2)}} = \frac{k_3 S\theta'^2_H}{k_{10}(1-\theta'_H)[R(1-\theta'_H) + k_9\theta'_H]} \quad (44)$$

Eq. (44) illustrating the ratio between the coverage of the chemisorbed half-hydrogenated intermediates and the coverage of the chemisorbed dehydrogenated intermediates also gives an indication if the reaction is following the half-hydrogenation route or the dehydrogenation route. This ratio has a high value when the coverage of chemisorbed hydrogen, θ'_H, is high and vice versa. Elimination of $\theta_{I(1)}$ and $\theta_{I(2)}$ by insertion of Eqs. (40) and (41) into Eqs. (30)–(35) gives the following expressions for the product generation rates:

$$r_B = \frac{1}{m}\frac{dc_B}{dt} = r_4 + r_{11} = \left[\frac{k_3k_4}{R(1-\theta'_H) + k_9\theta'_H} + \frac{k_{10}k_{11}}{S\theta'_H}\right]\theta_A\theta'_H(1-\theta'_H) \quad (45)$$

$$r_C = \frac{1}{m}\frac{dc_C}{dt} = r_5 + r_{12} = \left[\frac{k_3k_5}{R(1-\theta'_H) + k_9\theta'_H} + \frac{k_{10}k_{12}}{S\theta'_H}\right]\theta_A\theta'_H(1-\theta'_H) \quad (46)$$

$$r_D = \frac{1}{m}\frac{dc_D}{dt} = r_6 + r_{13} = \left[\frac{k_3k_6}{R(1-\theta'_H) + k_9\theta'_H} + \frac{k_{10}k_{13}}{S\theta'_H}\right]\theta_A\theta'_H(1-\theta'_H) \quad (47)$$

$$r_E = \frac{1}{m}\frac{dc_E}{dt} = r_7 + r_{14} = \left[\frac{k_3k_7}{R(1-\theta'_H) + k_9\theta'_H} + \frac{k_{10}k_{14}}{S\theta'_H}\right]\theta_A\theta'_H(1-\theta'_H) \quad (48)$$

$$r_U = \frac{1}{m}\frac{dc_U}{dt} = r_8 + r_{15} = \left[\frac{k_3k_8}{R(1-\theta'_H) + k_9\theta'_H} + \frac{k_{10}k_{15}}{S\theta'_H}\right]\theta_A\theta'_H(1-\theta'_H) \quad (49)$$

$$r_L = \frac{1}{m}\frac{dc_L}{dt} = r_9 = \frac{k_3k_9\theta'^2_H\theta_A}{R(1-\theta'_H) + k_9\theta'_H} \quad (50)$$

The coverage of **A**, θ_A, can be expressed via fraction of vacant sites. Insertion of

$$\theta_A = K_2\theta_0 c_A \quad (51)$$

into Eq. (29) and Eqs. (45)–(50) results in the consumption/generation rates

$$r_A = -\frac{1}{m}\frac{dc_A}{dt} = r_3 + r_{10} = [k_3\theta'_H + k_{10}(1-\theta'_H)]K_2\theta_0 c_A \quad (52)$$

$$r_B = \frac{1}{m}\frac{dc_B}{dt} = r_4 + r_{11} = \left[\frac{k_3k_4}{R(1-\theta'_H)+k_9\theta'_H} + \frac{k_{10}k_{11}}{S\theta'_H}\right] K_2\theta_0 c_A\theta'_H(1-\theta'_H) \quad (53)$$

$$r_C = \frac{1}{m}\frac{dc_C}{dt} = r_5 + r_{12} = \left[\frac{k_3k_5}{R(1-\theta'_H)+k_9\theta'_H} + \frac{k_{10}k_{12}}{S\theta'_H}\right] K_2\theta_0 c_A\theta'_H(1-\theta'_H) \quad (54)$$

$$r_D = \frac{1}{m}\frac{dc_D}{dt} = r_6 + r_{13} = \left[\frac{k_3k_6}{R(1-\theta'_H)+k_9\theta'_H} + \frac{k_{10}k_{13}}{S\theta'_H}\right] K_2\theta_0 c_A\theta'_H(1-\theta'_H) \quad (55)$$

$$r_E = \frac{1}{m}\frac{dc_E}{dt} = r_7 + r_{14} = \left[\frac{k_3k_7}{R(1-\theta'_H)+k_9\theta'_H} + \frac{k_{10}k_{14}}{S\theta'_H}\right] K_2\theta_0 c_A\theta'_H(1-\theta'_H) \quad (56)$$

$$r_U = \frac{1}{m}\frac{dc_U}{dt} = r_8 + r_{15} = \left[\frac{k_3k_8}{R(1-\theta'_H)+k_9\theta'_H} + \frac{k_{10}k_{15}}{S\theta'_H}\right] K_2\theta_0 c_A\theta'_H(1-\theta'_H) \quad (57)$$

$$r_L = \frac{1}{m}\frac{dc_L}{dt} = r_9 = \frac{k_3k_9K_2\theta_0\theta'^2_H c_A}{R(1-\theta'_H)+k_9\theta'_H} \quad (58)$$

The coverage of vacant sites, θ_0, in Eqs. (52)–(58) can be obtained from the balance equation

$$\theta_A + \theta_B + \theta_C + \theta_D + \theta_E + \theta_U + \theta_L + \theta_{I(1)} + \theta_{I(2)} + \theta_0 = 1 \quad (59)$$

After solving for coverages of respective reaction product from Eqs. (17)–(22),

$$\theta_B = \frac{\theta_0 c_B}{K_{16}} \quad (60)$$

$$\theta_C = \frac{\theta_0 c_C}{K_{17}} \quad (61)$$

$$\theta_D = \frac{\theta_0 c_D}{K_{18}} \quad (62)$$

$$\theta_E = \frac{\theta_0 c_E}{K_{19}} \quad (63)$$

$$\theta_U = \frac{\theta_0 c_U}{K_{20}} \quad (64)$$

$$\theta_L = \frac{\theta_0 c_L}{K_{21}} \quad (65)$$

and inserting Eq. (51), the coverages given by Eqs. (60)–(65), and the intermediate coverages given by Eqs. (40) and (41) into Eq. (59), one arrives at the following expression:

$$K_2\theta_0 c_A + \frac{\theta_0 c_B}{K_{16}} + \frac{\theta_0 c_C}{K_{17}} + \frac{\theta_0 c_D}{K_{18}} + \frac{\theta_0 c_E}{K_{19}} + \frac{\theta_0 c_U}{K_{20}} + \frac{\theta_0 c_L}{K_{21}} + \frac{k_3K_2\theta_0 c_A\theta'_H}{R(1-\theta'_H)+k_9\theta'_H} + \frac{k_{10}K_2\theta_0 c_A(1-\theta'_H)}{S\theta'_H} + \theta_0 = 1 \quad (66)$$

Eq. (66) can be written as

$$\theta_0\left[K_2c_A + \frac{c_B}{K_{16}} + \frac{c_C}{K_{17}} + \frac{c_D}{K_{18}} + \frac{c_E}{K_{19}} + \frac{c_U}{K_{20}} + \frac{c_L}{K_{21}} + \frac{k_3K_2c_A\theta'_H}{R(1-\theta'_H)+k_9\theta'_H} + \frac{k_{10}K_2c_A(1-\theta'_H)}{S\theta'_H} + 1\right] = 1 \quad (67)$$

hence the coverage of vacant sites, θ_0, can be expressed through reactant concentrations and coverage of hydrogen

$$\theta_0 = \frac{1}{\left[K_2c_A + \frac{c_B}{K_{16}} + \frac{c_C}{K_{17}} + \frac{c_D}{K_{18}} + \frac{c_E}{K_{19}} + \frac{c_U}{K_{20}} + \frac{c_L}{K_{21}} + \frac{k_3K_2c_A\theta'_H}{R(1-\theta'_H)+k_9\theta'_H} + \frac{k_{10}K_2c_A(1-\theta'_H)}{S\theta'_H} + 1\right]} \quad (68)$$

The consumption/generation rates are then given by

$$r_A = -\frac{1}{m}\frac{dc_A}{dt} = r_3 + r_{10} = [k_3\theta'_H + k_{10}(1-\theta'_H)]K_2c_A \cdot \frac{1}{D} = (r_A)^A \quad (69)$$

$$r_B = \frac{1}{m}\frac{dc_B}{dt} = r_4 + r_{11} = \left[\frac{k_3k_4}{R(1-\theta'_H)+k_9\theta'_H} + \frac{k_{10}k_{11}}{S\theta'_H}\right] K_2c_A\theta'_H(1-\theta'_H)\cdot\frac{1}{D} = (r_B)^A \quad (70)$$

$$r_C = \frac{1}{m}\frac{dc_C}{dt} = r_5 + r_{12} = \left[\frac{k_3k_5}{R(1-\theta'_H)+k_9\theta'_H} + \frac{k_{10}k_{12}}{S\theta'_H}\right] K_2c_A\theta'_H(1-\theta'_H)\cdot\frac{1}{D} = (r_C)^A \quad (71)$$

$$r_D = \frac{1}{m}\frac{dc_D}{dt} = r_6 + r_{13} = \left[\frac{k_3k_6}{R(1-\theta'_H)+k_9\theta'_H} + \frac{k_{10}k_{13}}{S\theta'_H}\right] K_2c_A\theta'_H(1-\theta'_H)\cdot\frac{1}{D} = (r_D)^A \quad (72)$$

$$r_E = \frac{1}{m}\frac{dc_E}{dt} = r_7 + r_{14} = \left[\frac{k_3k_7}{R(1-\theta'_H)+k_9\theta'_H} + \frac{k_{10}k_{14}}{S\theta'_H}\right] K_2 c_A \theta'^2_H (1-\theta'_H)\cdot\frac{1}{D} = (r_E)^A \quad (73)$$

$$r_U = \frac{1}{m}\frac{dc_U}{dt} = r_8 + r_{15} = \left[\frac{k_3k_8}{R(1-\theta'_H)+k_9\theta'_H} + \frac{k_{10}k_{15}}{S\theta'_H}\right] K_2 c_A \theta'^2_H (1-\theta'_H)\cdot\frac{1}{D} = (r_U)^A \quad (74)$$

$$r_L = \frac{1}{m}\frac{dc_L}{dt} = r_9 = \frac{k_3k_9K_2\theta'^2_H c_A}{R(1-\theta'_H)+k_9\theta'_H}\cdot\frac{1}{D} = (r_L)^A \quad (75)$$

where

$$D = K_2c_A + \frac{c_B}{K_{16}} + \frac{c_C}{K_{17}} + \frac{c_D}{K_{18}} + \frac{c_E}{K_{19}} + \frac{c_U}{K_{20}} + \frac{c_L}{K_{21}} + \frac{k_3K_2c_A\theta'_H}{R(1-\theta'_H)+k_9\theta'_H} + \frac{k_{10}K_2c_A(1-\theta'_H)}{S\theta'_H} + 1 \quad (76)$$

The variable θ'_H can be calculated as follows. The amount of chemisorbed hydrogen that desorbed from the ruthenium surface in the H_2-TPD measurements [7] while increasing the temperature from 100 °C to 600 °C is obtained by numerical integration of the H_2-TPD pattern ([7], shown in Fig. 3) in the corresponding temperature interval. This hydrogen amount can be considered as the total hydrogen uptake because in the kinetic isomerization experiments the catalyst was preactivated under hydrogen at 100 °C. The amount of hydrogen left on the catalyst surface after an increase of the temperature to the reaction temperature of 135 °C, 145 °C, 155 °C, or 165 °C is obtained in the same manner by integration under the H_2-TPD curve from consequent reaction temperature to 600 °C. The initial coverage of chemisorbed hydrogen, θ'_H, which depends on the reaction temperature, is estimated by dividing the amount of chemisorbed hydrogen left on the catalyst surface after a temperature increase to the reaction temperature used with the total hydrogen uptake. For example, the total hydrogen adsorption capacity was 1.77×10^{-4} mol H_2/g catalyst (related to the total catalyst mass) and the amount of chemisorbed hydrogen left on the metal surface after increasing the temperature to 165 °C was 1.10×10^{-4} mol H_2/g catalyst. Hence, at the reaction temperature of 165 °C, the initial coverage of chemisorbed hydrogen is 1.10×10^{-4} mol H_2/g catalyst/1.77×10^{-4} mol H_2/g catalyst = 0.62. The solvent *n*-decane does not act as a hydrogen transfer agent during the course of the kinetic runs, which leaves the chemisorbed hydrogen that is generated on the ruthenium surface in the catalyst preactivation step as the singe hydrogen source. Since the variable θ'_H in principle is dependent on the conversion of **A** to **L**, its value is obtained by calculating the required decrease of θ'_H for matching the observed generated amount of **L**, i.e. 1 mol of H_2 on the metal surface is needed for generation of 1 mol of **L**.

As described earlier, the selectivities toward compounds **B**, **C**, **D**, **E**, and **U** are rather independent on conversion as shown in Fig. 3. After division of the generation rates of **C**, **D**, **E**, and **U** given in Eqs. (71)–(74) by the generation rate of **B** given in Eq. (70), one arrives at expressions, which explicitly do not have unit time as a parameter,

$$Q_1 = \frac{r_C}{r_B} = \frac{dc_C}{dc_B} = \frac{N_C}{N_B} = \frac{k_3k_5S\theta'_H + k_{10}k_{12}[R(1-\theta'_H)+k_9\theta'_H]}{k_3k_4S\theta'_H + k_{10}k_{11}[R(1-\theta'_H)+k_9\theta'_H]} \quad (77)$$

$$Q_2 = \frac{r_D}{r_B} = \frac{dc_D}{dc_B} = \frac{N_D}{N_B} = \frac{k_3k_6S\theta'_H + k_{10}k_{13}[R(1-\theta'_H)+k_9\theta'_H]}{k_3k_4S\theta'_H + k_{10}k_{11}[R(1-\theta'_H)+k_9\theta'_H]} \quad (78)$$

$$Q_3 = \frac{r_E}{r_B} = \frac{dc_E}{dc_B} = \frac{N_E}{N_B} = \frac{k_3k_7S\theta'_H + k_{10}k_{14}[R(1-\theta'_H)+k_9\theta'_H]}{k_3k_4S\theta'_H + k_{10}k_{11}[R(1-\theta'_H)+k_9\theta'_H]} \quad (79)$$

$$Q_4 = \frac{r_U}{r_B} = \frac{dc_U}{dc_B} = \frac{N_U}{N_B} = \frac{k_3k_8S\theta'_H + k_{10}k_{15}[R(1-\theta'_H)+k_9\theta'_H]}{k_3k_4S\theta'_H + k_{10}k_{11}[R(1-\theta'_H)+k_9\theta'_H]} \quad (80)$$

where N_i denote mole fraction of compound i and Q_1–Q_4 are conversion independent constants. It should be noted that Eqs. (77)–(80) assume a constant hydrogen coverage at steady state, which can be justified by only some tiny generation of **L** in a hydrogen consuming step.

The kinetic constants, k, of stages 3–15 are assumed to follow the Arrhenius dependence

$$k = k^0 \exp\left(\frac{-E_a}{R_{gas}}\left(\frac{1}{T} - \frac{1}{T_{mean}}\right)\right) \quad (81)$$

In the expression above, k^0, E_a, R_{gas}, T, and T_{mean} denote frequency factor, activation energy, the gas constant, reaction temperature, and mean temperature of the experiments, correspondingly.

First of all, two essential and necessary simplifications of the model can be done. It is clear from Fig. 3 that the selectivities toward compounds **B**, **C**, **D**, **E**, **U**, and **L** are temperature independent. Such a result indicates that the catalytic stages 3–15 have the same activation energy E_a. Moreover, it is assumed that stages 16–21 describing desorption of reaction products, have the same equilibrium factors, i.e. $K_{16} = K_{17} = K_{18} = K_{19} = K_{20} = K_{21}$, because of the molecular similarity of these products. Thereafter, parameter estimation can be done on the mathematical model described by Eqs.

(69)–(76) and Eq. (81), which hereafter is referred to as model A.

However, model A, which as parameters contains the rate constants, k, of stages 3–15 as well as the equilibrium constants K_2 and K_{16}, is considerably over-parameterized. The model was thus split into two separate mechanisms. The role of the Horiuti–Polanyi mechanism [8] in isomerization and hydrogen of linoleic acid can be investigated by simply excluding stages 11–15 from the set of elementary stages. Similarly, the role of isomerization via the dehydrogenation pathway can be evaluated by excluding stages 4–8 from the set of elementary stages. The Horiuti–Polanyi pathway involving half-hydrogenated intermediates (stages 11–15 excluded) and the second pathway involving dehydrogenated intermediates (stages 4–8 excluded) are hereafter referred to as models B and C, respectively.

For model B, the consumption/generation rates are achieved by setting the kinetic constants $k_{11} = k_{12} = k_{13} = k_{14} = k_{15} = 0$ and the sum of kinetic constants $S = 0$ in Eqs. (69)–(80),

$$r_A = -\frac{1}{m}\frac{dc_A}{dt} = r_3 = k_3 K_2 c_A \theta'_H \cdot \frac{1}{D'} = (r_A)^B \quad (82)$$

$$r_B = \frac{1}{m}\frac{dc_B}{dt} = r_4 = \frac{k_3 k_4 K_2 c_A \theta'_H (1-\theta'_H)}{R(1-\theta'_H) + k_9 \theta'_H} \cdot \frac{1}{D'} = (r_B)^B \quad (83)$$

$$r_C = \frac{1}{m}\frac{dc_C}{dt} = r_5 = \frac{k_3 k_5 K_2 c_A \theta'_H (1-\theta'_H)}{R(1-\theta'_H) + k_9 \theta'_H} \cdot \frac{1}{D'} = (r_C)^B \quad (84)$$

$$r_D = \frac{1}{m}\frac{dc_D}{dt} = r_6 = \frac{k_3 k_6 K_2 c_A \theta'_H (1-\theta'_H)}{R(1-\theta'_H) + k_9 \theta'_H} \cdot \frac{1}{D'} = (r_D)^B \quad (85)$$

$$r_E = \frac{1}{m}\frac{dc_E}{dt} = r_7 = \frac{k_3 k_7 K_2 c_A \theta'_H (1-\theta'_H)}{R(1-\theta'_H) + k_9 \theta'_H} \cdot \frac{1}{D'} = (r_E)^B \quad (86)$$

$$r_U = \frac{1}{m}\frac{dc_U}{dt} = r_8 = \frac{k_3 k_8 K_2 c_A \theta'_H (1-\theta'_H)}{R(1-\theta'_H) + k_9 \theta'_H} \cdot \frac{1}{D'} = (r_U)^B \quad (87)$$

$$r_L = \frac{1}{m}\frac{dc_L}{dt} = r_9 = \frac{k_3 k_9 K_2 c_A \theta'^2_H}{R(1-\theta'_H) + k_9 \theta'_H} \cdot \frac{1}{D'} = (r_L)^B \quad (88)$$

where

$$D' = K_2 c_A + \frac{c_B}{K_{16}} + \frac{c_C}{K_{17}} + \frac{c_D}{K_{18}} + \frac{c_E}{K_{19}} + \frac{c_U}{K_{20}} + \frac{c_L}{K_{21}} + \frac{k_3 K_2 c_A \theta'_H}{R(1-\theta'_H) + k_9 \theta'_H} + 1 \quad (89)$$

The slopes of the mole fractions of compounds **C**, **D**, **E**, and **U**, versus the mole fraction of compound **B** shown in Fig. 3 are equal to the Q' factors, and thus these factors can be evaluated,

$$Q'_1 = \frac{r_C}{r_B} = \frac{dc_C}{dc_B} = \frac{N_C}{N_B} = \frac{k_5}{k_4} = \frac{A_5}{A_4} \quad (90)$$

$$Q'_2 = \frac{r_D}{r_B} = \frac{dc_D}{dc_B} = \frac{N_D}{N_B} = \frac{k_6}{k_4} = \frac{A_6}{A_4} \quad (91)$$

$$Q'_3 = \frac{r_E}{r_B} = \frac{dc_E}{dc_B} = \frac{N_E}{N_B} = \frac{k_7}{k_4} = \frac{A_7}{A_4} \quad (92)$$

$$Q'_4 = \frac{r_U}{r_B} = \frac{dc_U}{dc_B} = \frac{N_U}{N_B} = \frac{k_8}{k_4} = \frac{A_8}{A_4} \quad (93)$$

This allows essential simplification in the solving of the set of differential Eqs. (82)–(93), the remaining unknown parameters in model A are E_a, K_2, K_{16}, k_3^0, k_4^0, and k_9^0.

Regarding model C, on the other hand, the consumption/generation rates can be obtained by setting the kinetic constants $k_4 = k_5 = k_6 = k_7 = k_8 = 0$ and the sum of kinetic constants $R = 0$ in Eqs. (69)–(80),

$$r_A = -\frac{1}{m}\frac{dc_A}{dt} = r_3 + r_{10} = [k_3\theta'_H + k_{10}(1-\theta'_H)]K_2 c_A \cdot \frac{1}{D''} = (r_A)^C \quad (94)$$

$$r_B = \frac{1}{m}\frac{dc_B}{dt} = r_{11} = \frac{k_{10} k_{11} K_2 c_A (1-\theta'_H)}{S} \cdot \frac{1}{D''} = (r_B)^C \quad (95)$$

$$r_C = \frac{1}{m}\frac{dc_C}{dt} = r_{12} = \frac{k_{10} k_{12} K_2 c_A (1-\theta'_H)}{S} \cdot \frac{1}{D''} = (r_C)^C \quad (96)$$

$$r_D = \frac{1}{m}\frac{dc_D}{dt} = r_{13} = \frac{k_{10} k_{13} K_2 c_A (1-\theta'_H)}{S} \cdot \frac{1}{D''} = (r_D)^C \quad (97)$$

$$r_E = \frac{1}{m}\frac{dc_E}{dt} = r_{14} = \frac{k_{10} k_{14} K_2 c_A (1-\theta'_H)}{S} \cdot \frac{1}{D''} = (r_E)^C \quad (98)$$

$$r_U = \frac{1}{m}\frac{dc_U}{dt} = r_{15} = \frac{k_{10} k_{15} K_2 c_A (1-\theta'_H)}{S} \cdot \frac{1}{D''} = (r_U)^C \quad (99)$$

$$r_L = \frac{1}{m}\frac{dc_L}{dt} = r_9 = k_3 K_2 c_A \theta'_H \cdot \frac{1}{D''} = (r_L)^C \quad (100)$$

where

$$D'' = K_2 c_A + \frac{c_B}{K_{16}} + \frac{c_C}{K_{17}} + \frac{c_D}{K_{18}} + \frac{c_E}{K_{19}} + \frac{c_U}{K_{20}} + \frac{c_L}{K_{21}} + \frac{k_3 K_2 c_A}{k_9} + \frac{k_{10} K_2 c_A (1-\theta'_H)}{S\theta'_H} + 1 \quad (101)$$

An evaluation of the Q'' factors results in the following relation:

$$Q''_1 = \frac{r_C}{r_B} = \frac{dc_C}{dc_B} = \frac{N_C}{N_B} = \frac{k_{12}}{k_{11}} = \frac{A_{12}}{A_{11}} \quad (102)$$

$$Q_2'' = \frac{r_D}{r_B} = \frac{dc_D}{dc_B} = \frac{N_D}{N_B} = \frac{k_{13}}{k_{11}} = \frac{A_{13}}{A_{11}} \quad (103)$$

$$Q_3'' = \frac{r_E}{r_B} = \frac{dc_E}{dc_B} = \frac{N_E}{N_B} = \frac{k_{14}}{k_{11}} = \frac{A_{14}}{A_{11}} \quad (104)$$

$$Q_4'' = \frac{r_U}{r_B} = \frac{dc_U}{dc_B} = \frac{N_U}{N_B} = \frac{k_{15}}{k_{11}} = \frac{A_{15}}{A_{11}} \quad (105)$$

The remaining unknown parameters in the set of differential Eqs. (94)–(105) describing model B are E_a, K_2, K_{16}, k_3^0, k_9^0, k_{10}^0, and k_{11}^0. The values of the Q factors of models B and C are $Q_1' = Q_1'' = 0.58$, $Q_2' = Q_2'' = 0.38$, $Q_3' = Q_3'' = 0.08$, and $Q_4' = Q_4'' = 0.17$. The consumption/generation rates of compound i in models A, B, and C are hereafter referred to as $(r_i)^A$, $(r_i)^B$, and $(r_i)^C$, respectively. For example, the consumption rate of compound **A** (linoleic acid) in model B is denoted by $(r_A)^B$.

3.3. Parameter estimation

The systems of differential equations portraying models A (Eqs. (69)–(76) and Eq. (81)), B (Eqs. (82)–(93) and Eq. (81)), and C (Eqs. (94)–(105) and Eq. (81)) were in the parameter estimations solved numerically with the backward difference method by minimization of the sum of residual squares, SRS, with non-linear regression analysis using the Simplex and Levenberg–Marquardt optimization algorithms implemented in the software Modest [12]. The closeness of data and model-predicted values were measured with two criteria. If the mechanistic model formally is written

$$\begin{aligned} s &= f(x, \theta, c) \\ y_p &= g(s) \end{aligned} \quad (106)$$

where s, y_p, x, θ, and c denote state of the system, response variables, design variables, estimated parameters, and constants, the sum of residual squares is for the observed variables available, y_{ijk}, at experimental points, x_{jk}, defined by

$$\mathrm{SRS} = l(\theta) = ||y - y_p||_w^2 = \sum_{k=1}^{n\,\mathrm{sets}} \sum_{j=1}^{n\,\mathrm{obs}(k)} \sum_{i=1}^{ny\,\mathrm{data}(j,k)} (y_{ijk} - y_{pijk})^2 w_{ijk} \quad (107)$$

where w, giving the weight matrix for the observations, is equal to unity since all the response components are of comparable magnitude. In order to get the values of y and y_p as close as possible, the above sum was minimized with respect to θ using a step size of 0.1 and a value of 1×10^{-6} for both the absolute and relative tolerances of the Simplex and Levenberg–Marquardt optimizer (starting with Simplex and thereafter switching to Levenberg–Marquardt). The second criteria of the goodness the fit of the model was the degree of explanation, R^2,

$$R^2 = 100 \left(1 - \frac{||y - y_p||^2}{||y - \bar{y}_p||^2} \right) \% \quad (108)$$

where $\bar{y}$ is the average of the data points.

Taking a closer look at model A, which is given by Eqs. (69)–(76) and Eq. (81), it is seen that the first part of Eq. (69), the numerators of the first ratios of Eqs. (70)–(74), the numerator of Eq. (75), and the numerator of the second last ratio of Eq. (76) include the term k_3K_2. Additionally, the second part of Eq. (69), the numerators of the second ratios of Eqs. (70)–(74), and numerator of the last ratio of Eq. (76) contain the term $k_{10}K_2$. In model B, on the other hand, which is given by Eqs. (82)–(93) and Eq. (81), the term k_3K_2 appears in Eq. (82), in the numerators of the ratios of Eqs. (83)–(88), and in the numerator of the last ratio of Eq. (89). The factors k_3 and k_{10} are both involved in model C. Regarding model C, which is given by Eqs. (94)–(105) and Eq. (81), the term k_3K_2 appears in the first part of Eq. (94), in Eq. (100), and in the numerator of the second last ratio of Eq. (101), while the second part of Eq. (94), the numerators of Eqs. (95)–(99), and the numerator of the last ratio of Eq. (101) include the term $k_{10}K_2$. Further, the equilibrium constant K_{16} (which has the same value as equilibrium constants K_{17}, K_{18}, K_{19}, K_{20}, and K_{21}) comes into view in the denominator of Eq. (76) in model A, in the denominator of Eq. (89) in model B, and in the denominator of Eq. (101) in model C. These facts introduced crucial difficulties in the numerical solution of the systems of differential equations expressing the mathematical models. However, the problem can be solved in the following manner. From the actuality that the sum of all intermediate coverages, θ_A, θ_B, etc., of Eq. (59) is equal to unity, it is in turn required that the sum of all terms, $K_2\theta_0 c_A$, $\theta_0 c_B/K_{16}$, etc., included in Eq. (66) is equal to unity. In order to make parameter estimation possible, the values of the equilibrium factors must be chosen. It is reasonable, that the values of the individual terms $K_2\theta_0 c_A$, $\theta_0 c_B/K_{16}$, etc., involved in Eq. (66) at steady state have rather similar values due to the chemical similarity of adsorbed compounds Z**A**, Z**B**, Z**C**, Z**D**, Z**E**, Z**U**, Z**L**, and surface intermediates ZI(1) and ZI(2). Eq. (66) consists of 10 equally valuated terms whose sum is 1. Therefore, these values can be chosen to 0.1. Considering the magnitude of the concentrations of reactant and products, particularly the concentrations of compounds **A** and **B**, it is possible to get an indication of the values of the adsorption/desorption equilibrium constants K_2 and K_{16} from the constrains $K_2\theta_0 c_A = 0.1$ and $\theta_0 c_B/K_{16} = 0.1$, where $\theta_0 = 0.1$, since this in turn requires that the terms $K_2 c_A$ and c_B/K_{16} in Eq. (68) have values ≈1. Thus, in models A–C, these constants were fixed to $K_2 = 250\ \mathrm{dm^3\ mol^{-1}}$ and $K_{16} = 0.002\ \mathrm{mol\ dm^{-3}}$.

The results from the parameter value estimations are collected in Table 1. Model A showed the lowest SRS and highest R^2 of 0.3648×10^{-4} and 98.63%, respectively, for the three investigated mechanisms, but also very large estimated relative standard errors of the parameters, except for E_a, k_3, and k_{10}, due to the large number of parameters involved in the model. Model B showed a lower SRS and a higher R^2, i.e. 0.5139×10^{-4} and 98.08%, than those for model C, i.e. 0.1059×10^{-3} and 96.03%, respectively, and moreover the relative standard errors of the parameters of model B are reasonably low compared to those of model C. Sensitivity analysis performed on all combinations of the estimated parameters showed that the parameters in models B and C are still not well identified, except for the activation energy E_a, which showed a well identified minimum at corresponding estimated values of these parameters.

Comparisons of design and response linoleic acid concentration variables of the models are demonstrated in the parity

Table 1
Values of the estimated parameters of models A–C

Parameter	Estimated value			Estimated relative standard error (%)		
	A	B	C	A	B	C
E_a (J mol^{-1})	0.722×10^5	0.800×10^5	0.41×10^5	8.6	5.0	21.1
k_3^0 (mol g^{-1} min^{-1} dm^{-3})	0.580×10^{-4}	0.989×10^{-4}	0.721×10^{-2}	17.2	3.8	>100
k_4^0 (mol g^{-1} min^{-1} dm^{-3})	0.713×10^0	0.209×10^0	–	>100	16.2	–
k_5^0 (mol g^{-1} min^{-1} dm^{-3})	0.560×10^0	–	–	>100	–	–
k_6^0 (mol g^{-1} min^{-1} dm^{-3})	0.280×10^0	–	–	>100	–	–
k_7^0 (mol g^{-1} min^{-1} dm^{-3})	0.152×10^0	–	–	>100	–	–
k_8^0 (mol g^{-1} min^{-1} dm^{-3})	0.133×10^0	–	–	>100	–	–
k_9^0 (mol g^{-1} min^{-1} dm^{-3})	0.432×10^0	0.635×10^{-1}	0.427×10^0	>100	1.8	NaN
k_{10}^0 (mol g^{-1} min^{-1} dm^{-3})	0.417×10^{-4}	–	0.507×10^0	30.0	–	>100
k_{11}^0 (mol g^{-1} min^{-1} dm^{-3})	0.573×10^{-1}	–	0.188×10^{-4}	>100	–	19.0
k_{12}^0 (mol g^{-1} min^{-1} dm^{-3})	0.285×10^{-1}	–	–	>100	–	–
k_{13}^0 (mol g^{-1} min^{-1} dm^{-3})	0.259×10^{-1}	–	–	>100	–	–
k_{14}^0 (mol g^{-1} min^{-1} dm^{-3})	0.350×10^{-2}	–	–	>100	–	–
k_{15}^0 (mol g^{-1} min^{-1} dm^{-3})	0.161×10^{-1}	–	–	>100	–	–

Note: Model A—SRS = 0.3648×10^{-4}, R^2 = 98.63%; model B—SRS = 0.5139×10^{-4}, R^2 = 98.08%; model C—SRS = 0.1059×10^{-3}, R^2 = 96.03%.

diagrams given in Fig. 4 for all levels of the temperature and the catalysts mass that was used in the build-up of the models. The parity diagrams of observed and predicted concentrations of generated conjugated linoleic acid isomers and oleic acid followed the same pattern as the parity diagrams of the observed and predicted linoleic acid concentration. In Fig. 4, it can be seen that the predicted versus observed linoleic acid concentration dependence is better linearly collected for model B than those of model C.

Comparisons of all calculated concentrations with experimental data for linoleic acid isomerization on H_2-preactivated Ru/Al_2O_3 catalyst at a single temperature (165 °C) are demonstrated in Fig. 5. Model B clearly shows a better fit that model C, which could be taken to mean as an indication that the majority of **A** is converted via half-hydrogenated surface intermediates according to the Horiuti–Polanyi mechanism while only some **A** reacts to CLA via the second pathway involving dehydrogenated intermediates.

Let us briefly put models B and C side by side. Model C describing the dehydrogenation mechanism follows a reaction order that is close to zero with a fairly small deviation while model B describing the Horiuti–Polanyi mechanism has a higher reaction order, as seen in Fig. 5(b and c). As demonstrated in Fig. 5(a) in our previous paper [7], the kinetics of isomerization of linoleic acid over non-preactivated Ru/Al_2O_3 catalyst has a reaction order that is close to zero compared to that for isomerizations over H_2-preactivated Ru/Al_2O_3 catalyst with a higher reaction order. Moreover, as described earlier, a typical fashion for isomerizations on Ru/Al_2O_3 catalyst preactivated under a hydrogen atmosphere, is that the isomerization selectivity increases with conversion, as was shown in Fig. 5(b) in [7], since the hydrogenation reaction promoting chemisorbed hydrogen is consumed in the hydrogenation step under the course of the reaction. A non-preactivated catalyst, on the other hand, shows a more constant or conversion independent isomerization selectivity. Therefore, the predicted CLA isomer concentrations increase continuously in Fig. 5(c) (this paper) while the CLA generation rate approaches zero after some reaction time in Fig. 5(b). These two observations reflect the fact that isomerization kinetics on non-preactivated catalyst follows the dehydrogenation pathway while isomerization kinetics on H_2-preactivated catalyst predominantly follow the Horiuti–Polanyi mechanism, but only as long as chemisorbed hydrogen is available. Consequently, the prediction of model B, describing the Horiuti–Polanyi mechanism, follows the observed values with rather high accuracy in the beginning of the reaction, while a deviation appears after some conversion, as shown in Fig. 5(b), which is an expected trend. The fits of the two mechanistic models specify the foremost conclusion: when the coverage of chemisorbed hydrogen on the H_2-preactivated ruthenium surface has decreased after some conversion of **A**, the dehydrogenation mechanism starts to play a role.

A second possible explanation to the observed phenomena is the influence of catalyst deactivation. While comparing the values of the observed linoleic acid concentrations with the values of the predicted linoleic acid concentrations of models A–C, one more typical trend can be observed. Compared to the model predicted linoleic acid concentrations shown in Fig. 5 (solid lines), the observed linoleic acid concentrations (markers) drop faster in the beginning of the reaction, and thereafter the linoleic acid consumption rate decreases and a deviation appears, which could be attributed to some loss of catalytic activity with time. For this reason a deactivation step was inserted to the elementary stage mechanism and the concept was applied to each model.

3.4. Modeling of catalyst deactivation

The previous models assumed that the effectiveness of the catalyst in promoting the reaction would remain unchanged

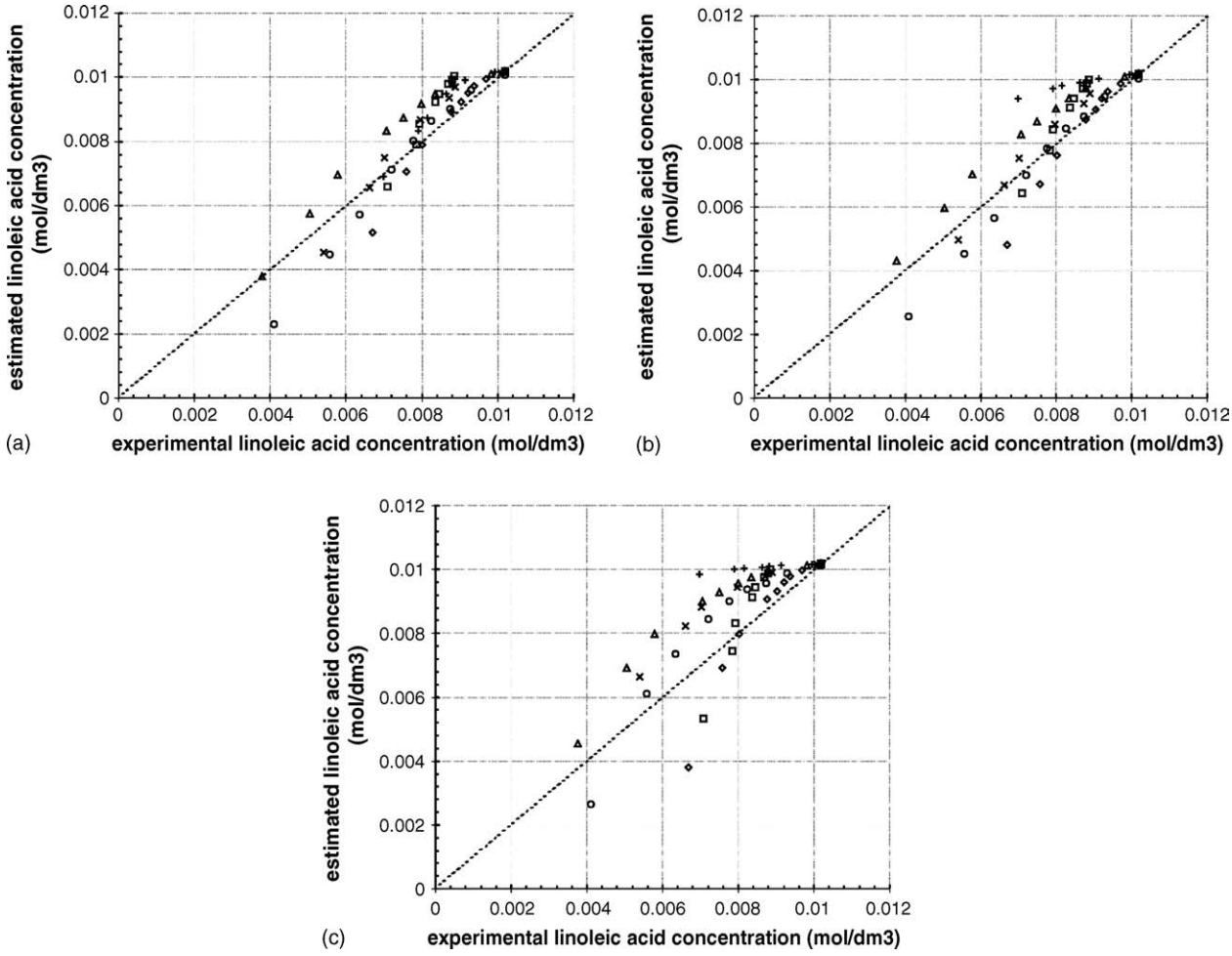

Fig. 4. Parity diagrams comparing observed linoleic acid concentration with predicted values of models (a) A, (b) B, and (c) C in isomerization of linoleic acid on H_2-preactivated Ru/Al_2O_3 catalyst at varied temperature and catalyst mass: (□) 135/0.8, (◇) 145/0.8, (△) 155/0.8, (◯) 165/0.8, (×) 165/0.4, (+) 165/0.2 °C/g. Other conditions same as Fig. 2.

with time, but still, as described in the previous paper [7], conversion, initial rate, and TOF, decreased with a factor of two as a second consecutive isomerization experiment was performed over the same regenerated Ru/Al_2O_3 sample, without any changes in BET specific surface area, pore volume distribution, or product selectivities. Thus, the reason for the observed deactivation is believed to lie within fouling of the active ruthenium sites or poisoning rather than irreversible plugging of pores by the heavy fatty acid molecules. The impact of deactivation such as structural modification of the surface due to sintering can be neglected at these mild conditions.

First of all, it is assumed, due to of the type of catalytic reaction, that the loss in activity occurs both through parallel deactivation and series deactivations. The key difference in these two forms of decay is that the deposition depends, respectively, on the concentration of reactant and the concentration products. However, no other reaction steps are observed than isomerization and hydrogenation of linoleic acid and due to the similarity of the chemical structures of the reactant and the reaction products, it is assumed that the reactant **A** as well as isomers **B**, **C**, **D**, **E**, **U** and the hydrogenation product **L** do all to the same extent produce side products, which deposits and deactivates the surface uniformly. Deactivation is caused only by reactant and product and since the total fatty acid concentration remains constant at any reaction time, this type of deactivation reduces to the "simple-to-treat" concentration independent deactivation and the profile of the total fatty acid concentration in the catalyst particle remain time independent. One arrives at expressions that although they are quite simple, they are general enough to embrace many of the decay equations used to date. The internal effectiveness factor was earlier proven to be 1 and the deposition will be uniformly distributed in the catalyst particle.

The activity, a, of a catalyst particle at any time is defined by Levenspiel [13] and Butt [14] as

$$a = \frac{-r_A}{-r_{A0}} \tag{109}$$

where $-r_A$ and $-r_{A0}$ denote the rate at which the catalyst converts reactant **A** and the rate of reaction of **A** with a fresh catalyst, respectively. Further, the rate of reaction of **A** is a function of temperature, concentration, and present activity of the catalyst. Similarly, the rate at which the catalyst deactivates may be a function of temperature and present state of the catalyst.

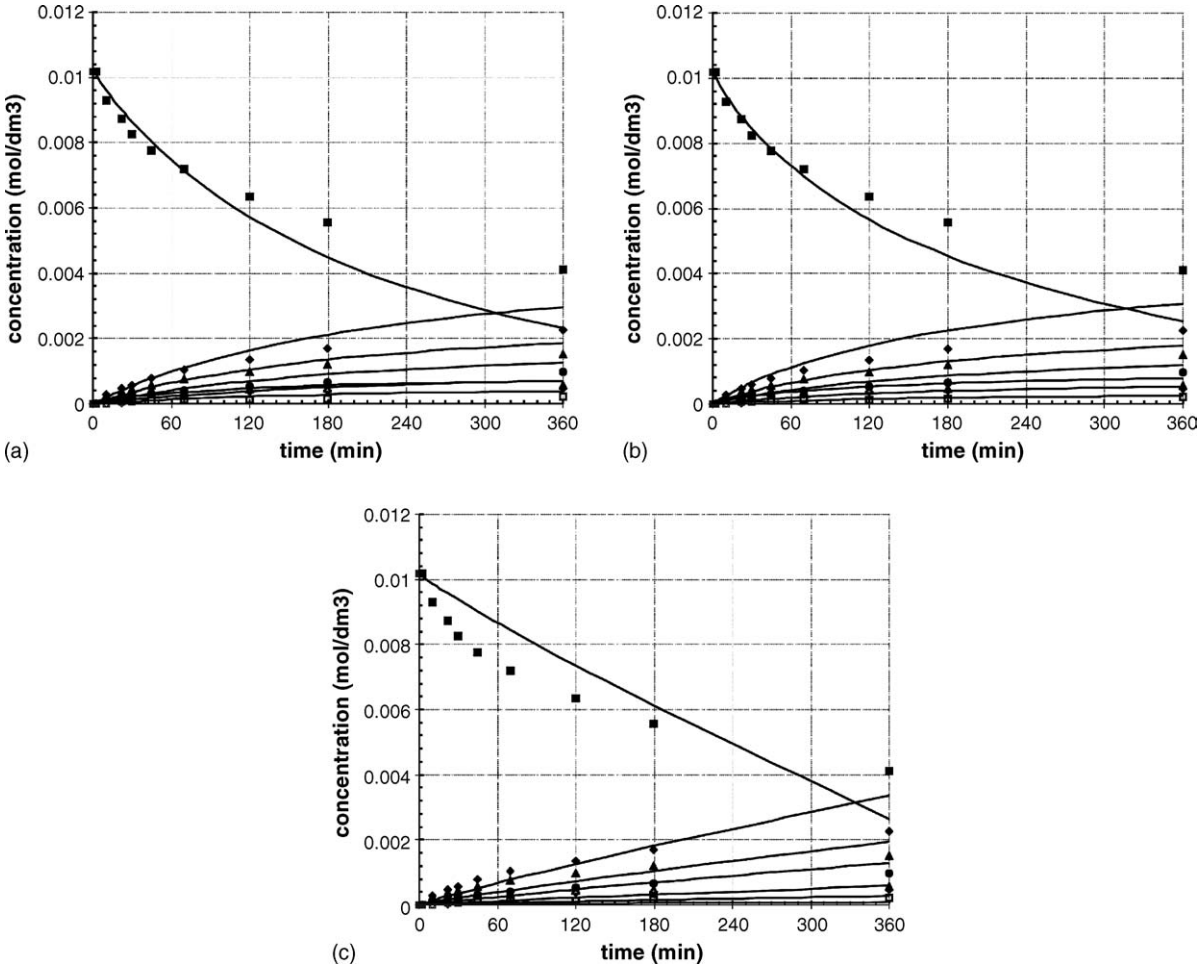

Fig. 5. Comparison of predictions of models (a) A, (b) B, and (c) C (solid lines) with experimental data (markers) for linoleic acid isomerization on H_2-preactivated Ru/Al_2O_3 catalyst at 165 °C: (■) **A**, (♦) **B**, (▲) **C**, (●) **D**, (□) **E**, (◊) **U**, (△) **L**. Catalyst mass, 0.8 g; stirring rate, 800 rpm. Other conditions same as Fig. 2.

The mathematical expression for the rate of deactivation can be written as

$$-\frac{da}{dt} = k_d a^d \tag{110}$$

where d is the order of deactivation. The deactivation constant k_d follows the dependence

$$k_d = k_{d0} \exp\left(\frac{-E_d}{R_{gas}}\left(\frac{1}{T} - \frac{1}{T_{mean}}\right)\right) \tag{111}$$

where k_{d0} and E_d describe the frequency factor and the activation energy or temperature dependency of the deactivation. The constants d, k_{d0}, and E_d are because of the similarity of the chemical structures of all involved compounds assumed to be the same, correspondingly, for each catalytic stage in the reaction mechanism.

If the initial activity $a_0 = 1$ and the order of deactivation $d \neq 1$, integration of Eq. (110) gives the expression

$$a = [1 + (d-1)k_d t]^{1/1-d} \tag{112}$$

Deactivation functions used in the modeling obtained by analytical solution, i.e. integration, of Eq. (110) for zero, first, second, and third order of deactivation are collected in Table 2.

In the parameter estimation procedure, the same assumptions and numerical methods are used as described above in the previous chapter. The new parameters are d, k_{d0}, and E_d, and the single difference is that in terms of kinetics, after inserting the mathematical expression for catalyst deactivation, Eqs. (69)–(75) model A becomes

$$r_A = (r_A)^A \cdot a \tag{113}$$

$$r_B = (r_B)^A \cdot a \tag{114}$$

Table 2
Deactivation functions obtained by integration of Eq. (110)

Order of deactivation	Analytical solution of Eq. (110)	Initial activity $a_0 = 1$ (used in models)
$d = 0$	$a = a_0 - k_d t$	$a = 1 - k_d t$
$d = 1$	$a = a_0 \exp(-k_d t)$	$a = \exp(-k_d t)$
$d = 2$	$a = \frac{1}{k_d t + \frac{1}{a_0}}$	$a = \frac{1}{k_d t + 1}$
$d = 3$	$a = \frac{1}{\sqrt{2k_d t + \frac{1}{a_0^2}}}$	$a = \frac{1}{\sqrt{2k_d t + 1}}$

Table 3
Values of the estimated parameters of models A(1), A(2), and A(3)

Parameter	Estimated value			Estimated relative standard error (%)		
	A(1)	A(2)	A(3)	A(1)	A(2)	A(3)
E_a (J mol^{-1})	0.526×10^5	0.765×10^5	0.651×10^5	11.5	16.9	NaN
k_3^0 (mol g^{-1} min^{-1} dm^{-3})	0.479×10^{-4}	0.960×10^{-4}	0.547×10^{-4}	45.6	52.5	NaN
k_4^0 (mol g^{-1} min^{-1} dm^{-3})	0.590×10^0	0.501×10^{-2}	0.167×10^2	>100	>100	NaN
k_5^0 (mol g^{-1} min^{-1} dm^{-3})	0.652×10^0	0.428×10^{-2}	0.135×10^2	>100	>100	NaN
k_6^0 (mol g^{-1} min^{-1} dm^{-3})	0.556×10^{-1}	0.188×10^{-2}	0.694×10^1	>100	>100	NaN
k_7^0 (mol g^{-1} min^{-1} dm^{-3})	0.795×10^{-1}	0.105×10^{-2}	0.276×10^1	>100	>100	NaN
k_8^0 (mol g^{-1} min^{-1} dm^{-3})	0.168×10^{-1}	0.102×10^{-6}	0.381×10^1	>100	>100	NaN
k_9^0 (mol g^{-1} min^{-1} dm^{-3})	0.101×10^1	0.395×10^{-2}	0.112×10^2	>100	>100	NaN
k_{10}^0 (mol g^{-1} min^{-1} dm^{-3})	0.158×10^{-3}	0.122×10^{-3}	0.472×0^{-4}	21.0	31.1	NaN
k_{11}^0 (mol g^{-1} min^{-1} dm^{-3})	0.212×10^0	0.672×10^{-1}	0.223×10^2	>100	>100	NaN
k_{12}^0 (mol g^{-1} min^{-1} dm^{-3})	0.116×10^0	0.342×10^{-1}	0.113×10^2	>100	>100	NaN
k_{13}^0 (mol g^{-1} min^{-1} dm^{-3})	0.101×10^0	0.299×10^{-1}	0.965×10^1	>100	>100	NaN
k_{14}^0 (mol g^{-1} min^{-1} dm^{-3})	0.204×10^{-1}	0.311×10^{-2}	0.187×10^1	>100	>100	NaN
k_{15}^0 (mol g^{-1} min^{-1} dm^{-3})	0.601×10^{-1}	0.247×10^{-1}	0.550×10^1	>100	>100	NaN
k_{d0} (min^{-1})	0.102×10^{-1}	0.245×10^{-1}	0.548×10^{-2}	7.9	28.6	NaN
E_d (J mol^{-1})	0.100×10^5	0.100×10^5	0.999×10^4	89.3	>100	NaN

Note: Model A(1)—SRS = 0.1714×10^{-4}, R^2 = 99.36%; model A(2)—SRS = 0.2022×10^{-4}, R^2 = 99.24%; model A(3)—SRS = 0.3617×10^{-3}, R^2 = 98.65%.

Table 4
Values of the estimated parameters of models B(0), B(1), B(2), and B(3)

Parameter	Estimated value				Estimated relative standard error (%)			
	B(0)	B(1)	B(2)	B(3)	B(0)	B(1)	B(2)	B(3)
E_a (J mol^{-1})	0.798×10^5	0.800×10^5	0.736×10^5	0.800×10^5	7.4	9.3	13.6	NaN
k_3^0 (mol g^{-1} min^{-1} dm^{-3})	0.138×10^{-3}	0.157×10^{-3}	0.184×10^{-3}	0.989×10^{-4}	6.3	8.3	12.1	NaN
k_4^0 (mol g^{-1} min^{-1} dm^{-3})	0.345×10^0	0.639×10^{-1}	0.160×10^{-1}	0.332×10^{-1}	14.8	14.5	14.4	NaN
k_9^0 (mol g^{-1} min^{-1} dm^{-3})	0.988×10^{-1}	0.181×10^{-1}	0.447×10^{-2}	0.101×10^{-1}	1.6	1.7	1.9	NaN
k_{d0} (min^{-1})	0.375×10^{-2}	0.738×10^{-2}	0.175×10^{-1}	0.140×10^{-2}	10.3	15.7	26.4	NaN
E_d (J mol^{-1})	0.998×10^4	0.100×10^5	0.100×10^5	0.100×10^5	>100	>100	>100	NaN

Note: Model B(0)—SRS = 0.4259×10^{-4}, R^2 = 98.40%; model B(1)—SRS = 0.4117×10^{-4}, R^2 = 98.46%; model B(2)—SRS = 0.3992×10^{-3}, R^2 = 98.51%; model B(3)—SRS = 0.5140×10^{-3}, R^2 = 98.08%.

Table 5
Values of the estimated parameters of models C(1), C(2), and C(3)

Parameter	Estimated value			Estimated relative standard error (%)		
	C(1)	C(2)	C(3)	C(1)	C(2)	C(3)
E_a (J mol^{-1})	0.400×10^5	0.420×10^5	0.400×10^5	12.2	18.6	NaN
k_3^0 (mol g^{-1} min^{-1} dm^{-3})	0.251×10^{-4}	0.357×10^{-4}	0.143×10^{-4}	25.9	37.5	NaN
k_9^0 (mol g^{-1} min^{-1} dm^{-3})	0.660×10^{-2}	0.433×10^{-2}	0.102×10^{-1}	>100	>100	NaN
k_{10}^0 (mol g^{-1} min^{-1} dm^{-3})	0.204×10^{-3}	0.288×10^{-3}	0.952×10^{-4}	24.1	36.8	NaN
k_{11}^0 (mol g^{-1} min^{-1} dm^{-3})	0.319×10^{-2}	0.309×10^{-2}	0.117×10^{-1}	44.0	47.5	NaN
k_{d0} (min^{-1})	0.107×10^{-1}	0.390×10^{-1}	0.695×10^{-2}	9.5	23.2	NaN
E_d (J mol^{-1})	0.100×10^5	0.240×10^4	0.997×10^4	81.0	>100	NaN

Note: Model C(1)—SRS = 0.1683×10^{-4}, R^2 = 99.37%; model C(2)—SRS = 0.1379×10^{-4}, R^2 = 99.48%; model C(3)—SRS = 0.3938×10^{-3}, R^2 = 98.53%.

$$r_C = (r_C)^A \cdot a \quad (115)$$

$$r_D = (r_D)^A \cdot a \quad (116)$$

$$r_E = (r_E)^A \cdot a \quad (117)$$

$$r_U = (r_U)^A \cdot a \quad (118)$$

$$r_L = (r_L)^A \cdot a \quad (119)$$

Including the catalyst deactivation expression in model B, the set of differential Eqs. (82)–(88) becomes

$$r_A = (r_A)^B \cdot a \quad (120)$$

$$r_B = (r_B)^B \cdot a \quad (121)$$

$$r_C = (r_C)^B \cdot a \quad (122)$$

$$r_D = (r_D)^B \cdot a \quad (123)$$

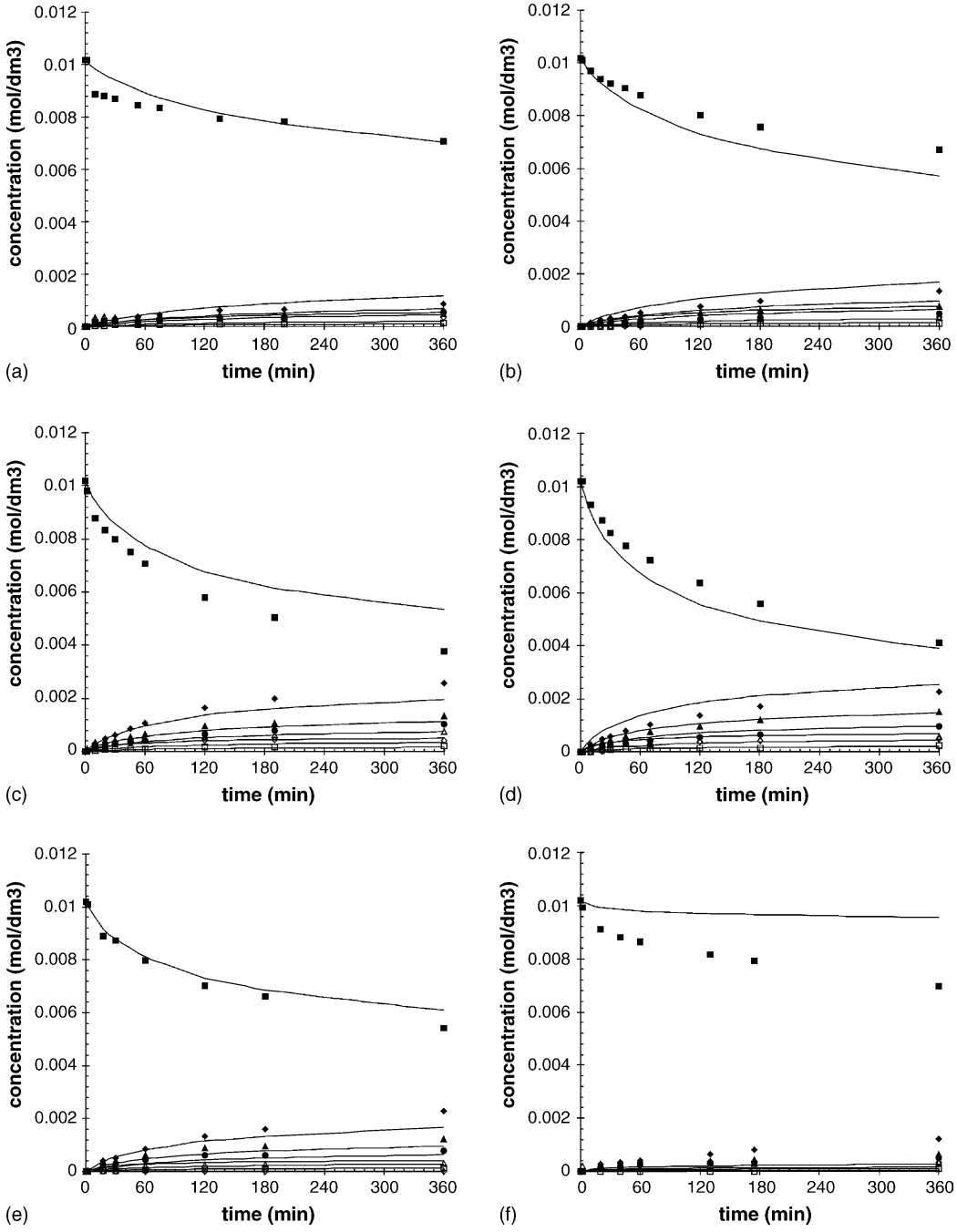

Fig. 6. Comparison of predictions of mathematical model B(2) (solid lines) with experimental data (markers) for linoleic acid isomerization on H_2-preactivated Ru/Al_2O_3 catalyst at varied levels of reaction temperature and catalyst mass: (■) **A**, (♦) **B**, (▲) **C**, (●) **D**, (□) **E**, (◇) **U**, (△) **L**. (a) 135/0.8, (b) 145/0.8, (c) 155/0.8, (d) 165/0.8, (e) 165/0.4, and (f) 165/0.2 °C/g. Other conditions same as Fig. 2.

$$r_E = (r_E)^B \cdot a \quad (124)$$

$$r_U = (r_U)^B \cdot a \quad (125)$$

$$r_L = (r_L)^B \cdot a \quad (126)$$

As the final point, after including the expression of the new concept model C, the set of differential Eqs. (94)–(100) changes to

$$r_A = (r_A)^C \cdot a \quad (127)$$

$$r_B = (r_B)^C \cdot a \quad (128)$$

$$r_C = (r_C)^C \cdot a \quad (129)$$

$$r_D = (r_D)^C \cdot a \quad (130)$$

$$r_E = (r_E)^C \cdot a \quad (131)$$

$$r_U = (r_U)^C \cdot a \quad (132)$$

$$r_L = (r_L)^C \cdot a \quad (133)$$

After involving mathematical expressions describing deactivation in models A–C, they are hereby referred to as models A(*d*), B(*d*), and C(*d*). For example, after applying Eqs. (110) and (111) to model A with the order of deactivation

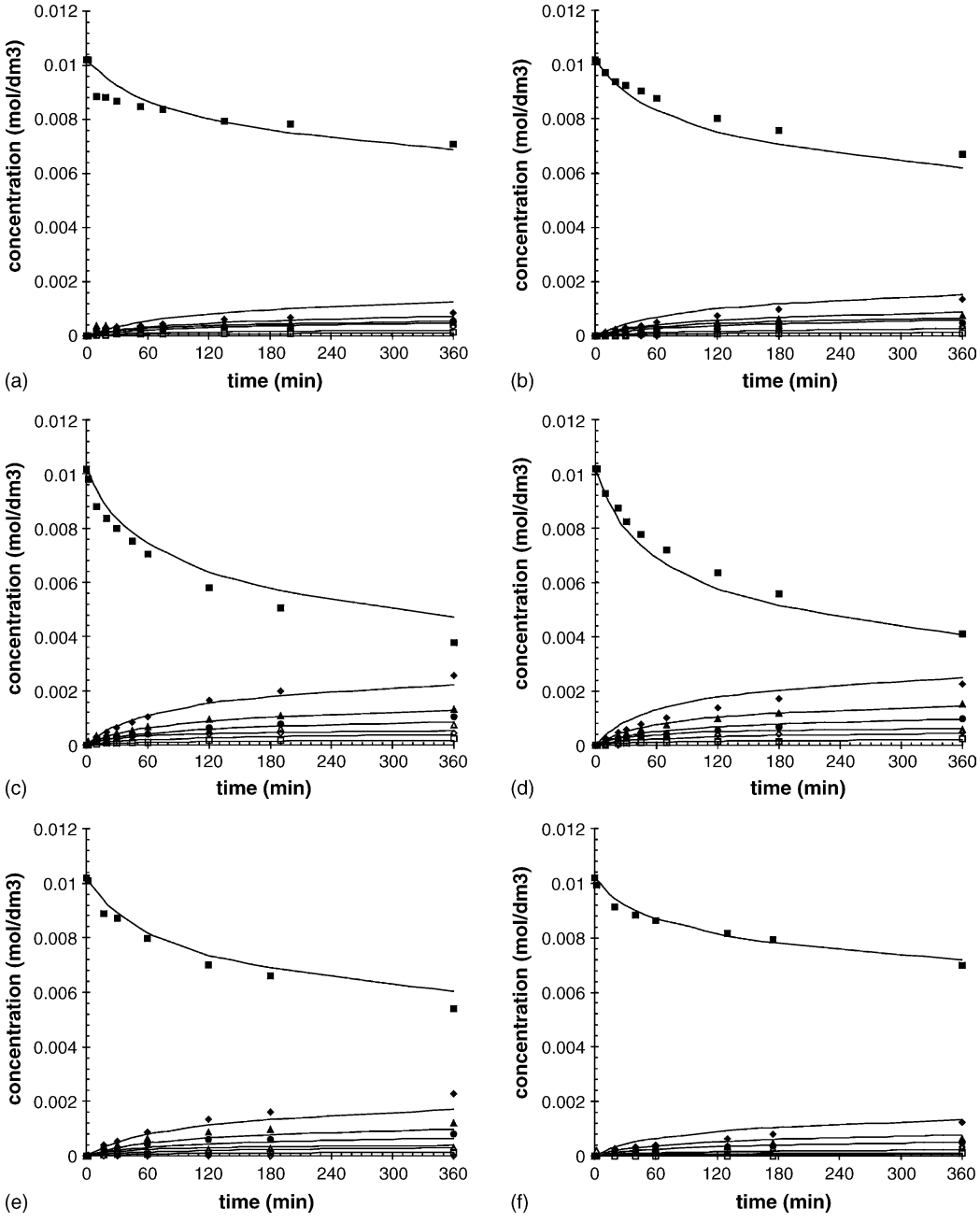

Fig. 7. Comparison of predictions of mathematical model C(2) (solid lines) with experimental data (markers) for linoleic acid isomerization on H_2-preactivated Ru/Al_2O_3 catalyst at varied levels of reaction temperature and catalyst mass: (■) **A**, (♦) **B**, (▲) **C**, (●) **D**, (□) **E**, (◊) **U**, (△) **L**. (a) 135/0.8, (b) 145/0.8, (c) 155/0.8, (d) 165/0.8, (e) 165/0.4, (f) 165/0.2 °C/g. Other conditions same as Fig. 2.

$d = 0$, it is referred to as model A(0). Similarly, model B with second order of deactivation is denoted by B(2), etc. Values of estimated kinetic parameters, estimated relative standard error of the parameters, sum of residual squares (SRS), and degree of explanation (R2) after a parameter estimation of models A(d), B(d), and C(d) for $d = 0$, 1, 2, and 3 are presented in Tables 3–5.

All models A(1), A(2), and A(3) including deactivation steps showed a lower SRS term and a higher R^2 term than model A as presented in Table 3. The degree of explanation terms were 99.36%, 99.24%, and 98.65%, and the sum of residual squared were 0.1714×10^{-4}, 0.2022×10^{-4}, and 0.3617×10^{-3} for models A(1), A(2), and A(3), respectively, while model A only showed an R^2 of 98.63% and an SRS of 0.3648×10^{-4}. Unfortunately, it was not possible to solve the systems of differential equations representing model A(0) numerically. The A(d) models, specifically model A(1) due to its lowest sum of squares, also gave a better fit of experimental and estimated component concentrations than model A. It still cannot be concluded based only on data fitting that the reason for the better quality of model A(1) would be that the linoleic acid isomerization reaction follows the reaction mechanism corresponding to this model, that is a combination of the Horiuti–Polanyi mechanism and the dehydrogenation mechanism. The fact that the two kinetic term k_{d0} and E_d have been included in the models A(d) contributes to their lower SRS and better fit. As shown in Table 3, the estimated relative standard errors of the parameters of model A(d) are far too large for any attempt to correlate these models to observed kinetic regularities. The A(d) systems have too many parameters and too polynomial nature for achieving low estimated relative standard errors of the kinetic parameters.

Considering the B(d) systems, the degree of explanation terms were 98.40%, 98.46%, 98.51%, and 98.08%, and the sum of residual squared were 0.4259×10^{-4}, 0.4117×10^{-4}, 0.3992×10^{-3}, and 0.5140×10^{-3}, for $d = 0$, 1, 2, and 3, respectively, while model B showed an R^2 of 98.08% and an SRS of 0.5139×10^{-4}. As expected from the statistic values, model B(2) gave a better fit of experimental and estimated concentrations than model B, B(0), B(1), and B(3) and moreover a promising indication is that, as shown in Table 4, the estimated relative standard errors of the parameters of models B(0), B(1), and B(2) are reasonably low.

Although the Simplex and Levenberg–Marquardt optimized could not solve Eq. (107) for model C(0), model C was dramatically improved when the first, second, and third order deactivation functions were applied to it. Model C initially showed rather low SRS and R^2 terms, i.e. 0.1059×10^{-3} and 96.03%, respectively, which are improved to 0.1683×10^{-4} and 99.37% for $d = 1$, 0.1379×10^{-4} and 99.48% for $d = 2$, as well as 0.3938×10^{-3} and 98.53% for $d = 3$. Model C(2) gave the best fit of the C(d) systems but model C(1) is almost as good and as demonstrated in Table 5, models C(1) and C(2) both showed rather low estimated relative standard errors of the parameters compared to model C.

Model B(2) has the lowest SRS of the B(d) systems while model C(2) has the lowest SRS of the C(d) systems, indicating the catalyst deactivation of the isomerization reaction is of second order. From a statistical point of view it might be difficult to elucidate whether model B(2) or C(2) is more consistent with concrete mechanistic data. Model B(2) describes isomerization and hydrogenation of linoleic acid via half-hydrogenated intermediates according to the Horiuti–Polanyi mechanism with second order of catalyst deactivation. Model C(2) including second order of catalyst deactivation, on the other hand, portrays isomerization of linoleic acid via dehydrogenated intermediates according to the mechanism described above as well as hydrogenation of linoleic acid via half-hydrogenated intermediates according to the Horiuti–Polanyi mechanism. We are slightly contradicting with ourselves as we were emphasizing importance of both routes. Both models very well accomplish the two criteria for closeness of data and model-predicted values and the systems have quite low relative parameter standard errors. However, two more facts can be observed. From Tables 4 and 5 it can be seen that model B(2) has an SRS of 0.3992×10^{-3} and an R^2 term of 98.51%. Corresponding values of model C(2) are 0.1399×10^{-4} and $R^2 = 99.48\%$. Moreover, while comparing experimental data and model-predicted values, it can be observed that model B(2) cannot fulfill the criteria of the goodness the fit for all conditions.

Comparisons of all predicted concentrations with experimental data for linoleic acid isomerization on H_2-preactivated Ru/Al_2O_3 catalyst at all conditions that were used in the build-up of these models are demonstrated in Figs. 6 (model B(2)) and 7 (model C(2)). While model C(2) shows a more or less perfect data fitting as seen in Fig. 7, some deviations between predicted and observed concentration values of model B(2) appear as the catalyst mass is lower via the half amount to the quarter amount of catalyst as seen in Fig. 6(f). This is an indication that of the investigated models, the mechanistic data of

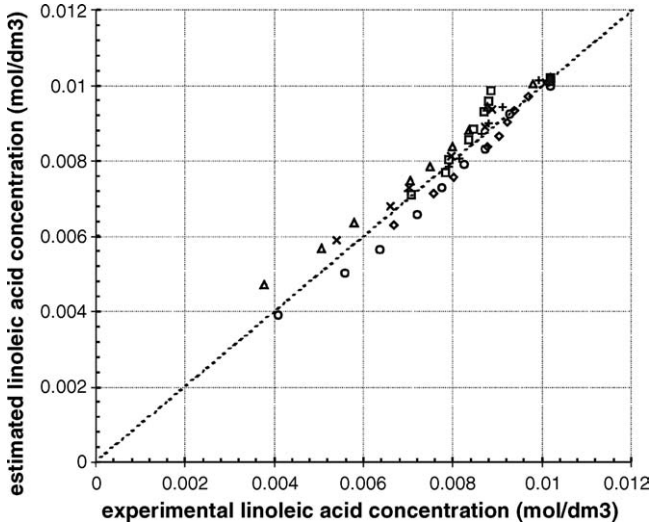

Fig. 8. Parity diagram comparing observed linoleic acid concentration with predicted values of model C(2) in isomerization of linoleic acid on H_2-preactivated Ru/Al_2O_3 catalyst at varied temperature and catalyst mass: (□) 135/0.8, (◊) 145/0.8, (△) 155/0.8, (○) 165/0.8, (×) 165/0.4, (+) 165/0.2 °C/g. Other conditions same as Fig. 2.

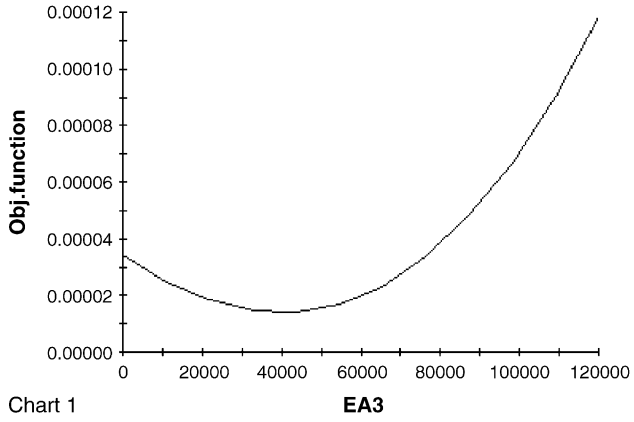

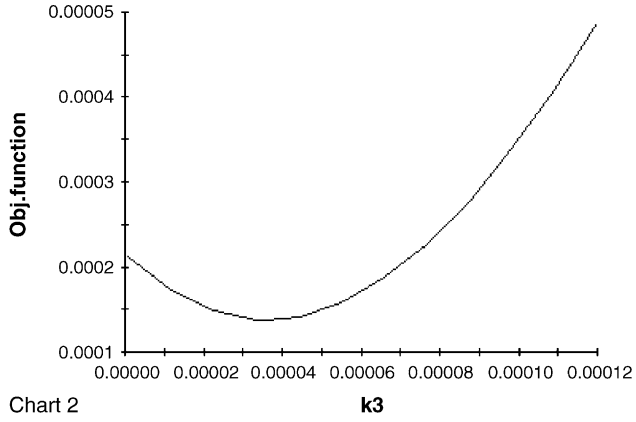

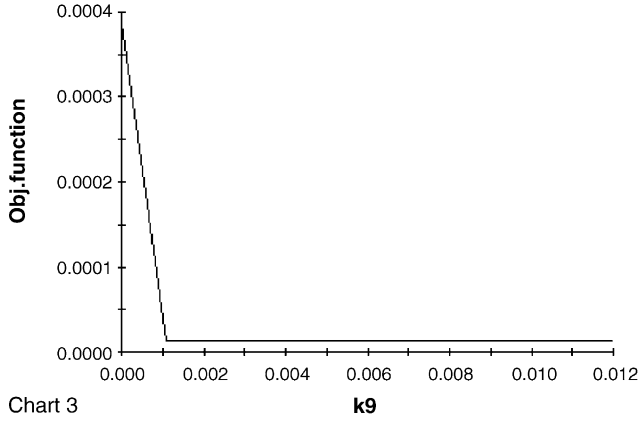

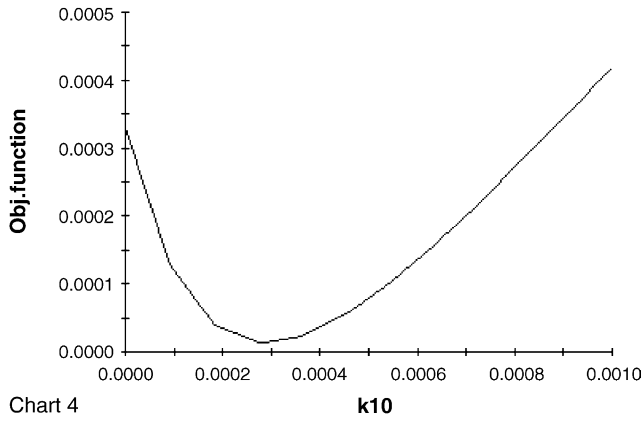

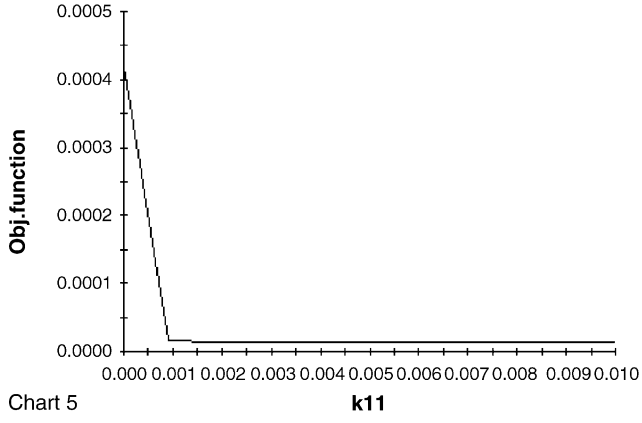

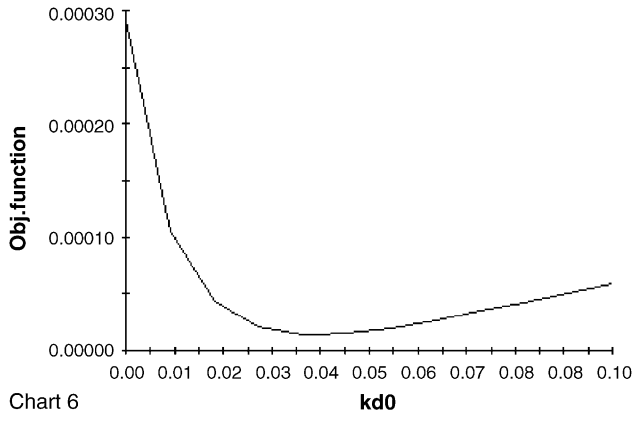

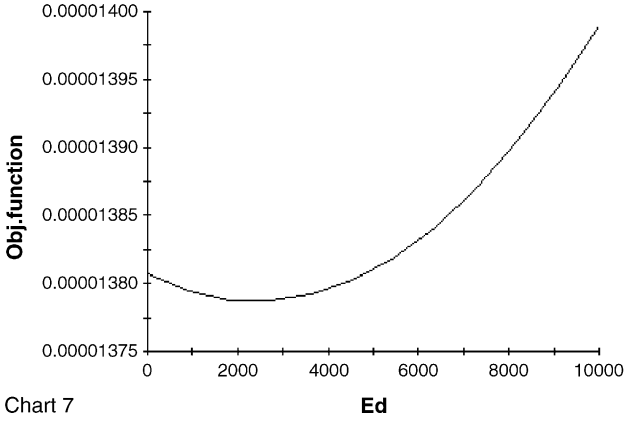

Fig. 9. Objective function (sum of residual squares) vs. the parameters (a) E_a, (b) k_3^0, (c) k_9^0, (d) k_{10}^0, (e) k_{11}^0, (f) k_{d0}, and (g) E_d of model C(2).

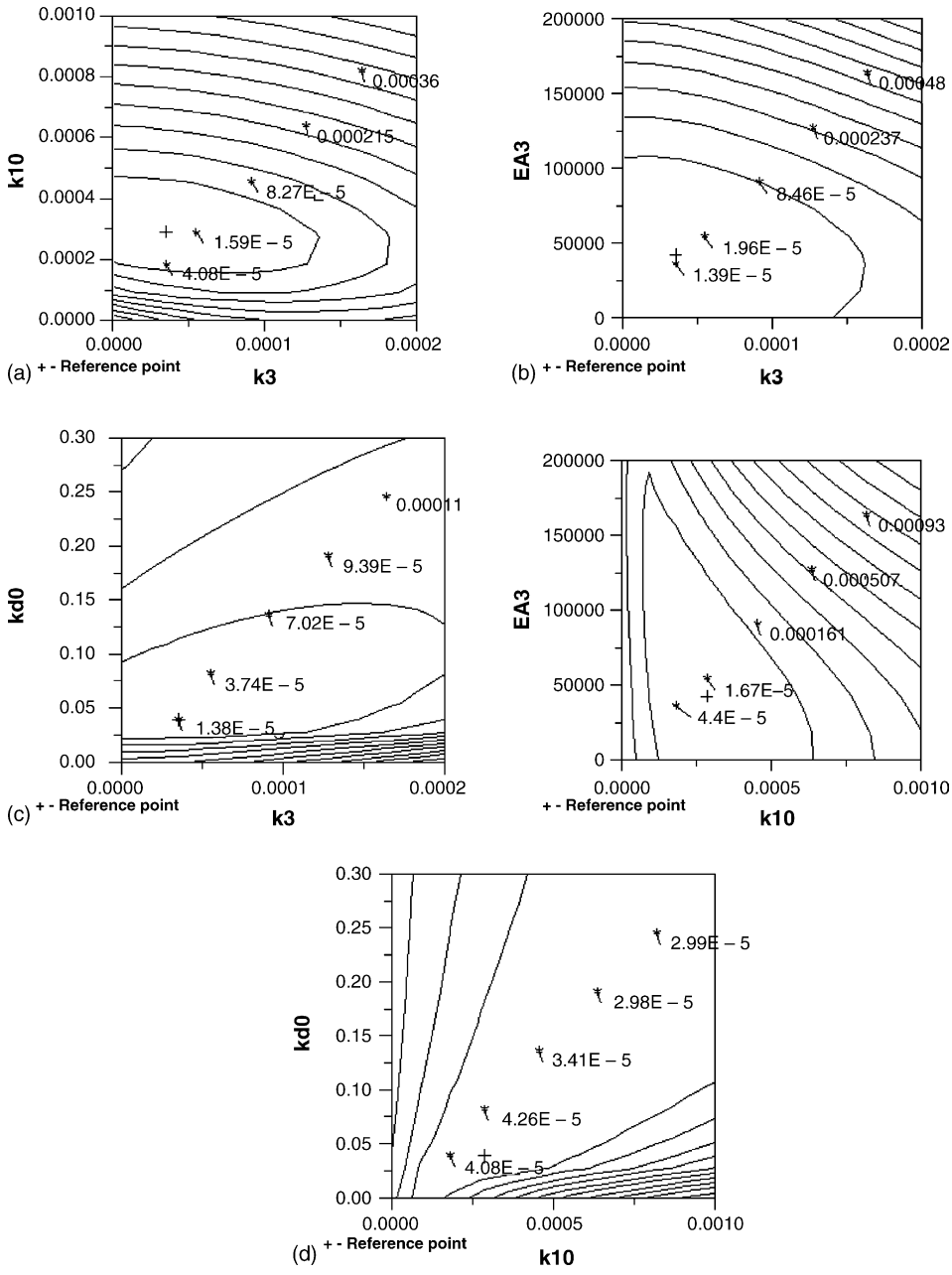

Fig. 10. Contour plots of the sum of residual squares from sensitivity analysis of some parameters of model C(2). (a) k_3^0 vs. k_{10}^0, (b) k_3^0 vs. E_a, (c) k_3^0 vs. k_{d0}, (d) k_{10}^0 vs. E_a, and (e) k_{10}^0 vs. k_{d0}.

model C(2) is most consistent and observed kinetic regularities.

A comparisons of design and response variables of model C(2) is demonstrated in the parity diagram given in Fig. 8 for all levels of the temperature and the catalysts mass that was used in the build-up of the models. It can be seen that the predicted versus observed linoleic acid concentration dependence rather linearly collected.

The SRS values as a function of the parameters of model C(2) was obtained by sensitivity analysis. As can be seen in Fig. 9, E_a, k_3^0, and k_{10}^0, which also have low values of the relative parameter standard error (Table 5, entries 1, 2, and 4) compared to, for example, k_9^0 (Table 5, entry 3), showed a rather sharp minima of the objective function.

Thus, the sensitivity plots of these parameters indicate a relatively low parameter correlation, as Fig. 10 demonstrates. The sensitivity plots of the parameters E_a and k_{d0} versus k_3^0 in Fig. 10(b and c) are quite similar to k_{10}^0 versus k_3^0 in Fig. 10a). All sensitivity analyses, in which parameters k_9^0 and k_{11}^0 where involved, showed somewhat higher parameter correlation. Moreover, most of the minima of the objective functions of the parameters of models A(1) and B(2) not well defied.

4. Conclusions

Isomerization of linoleic acid to *cis*-9,*trans*-11-conjugated linoleic acid and *trans*-10,*cis*-12-conjugated linoleic acid on

H_2-preactivated as well as non-preactivated Ru/Al_2O_3 catalyst was studied at 135–165 °C under kinetic control in slurry reactor under atmospheric pressure in *n*-decane solution. The isomerization and hydrogenation kinetics was mechanistically modeled based on a proposed elementary step reaction network to get information on the role of chemisorbed hydrogen. The catalyst was characterized by using nitrogen adsorption, X-ray photoelectron spectroscopy, scanning electron microscopy-energy dispersive X-ray analysis, and temperature programmed desorption of hydrogen techniques. Over such catalyst and at the conditions used, the reaction scheme involves competitive double bond migration of linoleic acid to CLA isomers as well as hydrogenation of linoleic acid to oleic acid. These competing parallel steps are through a complex relation strongly affected by chemisorbed hydrogen on the Ru surface. The isomerization rate was enhanced by catalyst preactivation under hydrogen, but increased hydrogen coverage on the Ru surface also restrained the isomerization selectivity. The total reaction network with two mechanisms combined (model A) was split into two separate mechanisms (models B and C, e.g. hydrogen addition – hydrogen abstraction and dehydrogenation – hydrogen addition, respectively) to make parameter estimation more transparent and investigate the role of hydrogen on the Ru surface. The role of the Horiuti–Polanyi mechanism involving half-hydrogenated intermediates in isomerization and hydrogen of linoleic acid (model B) was compared with the role of isomerization via a dehydrogenation pathway (model C) involving dehydrogenated intermediates. Model B showed a lower SRS and a higher R^2 than those for model C and moreover the relative standard errors of the parameters of model B are reasonably low compared to those of model C. It is possible that over a catalyst, which is previously preactivated under hydrogen, the isomerization and hydrogenation initially occur through the Horiuti–Polanyi mechanism. When the coverage of chemisorbed hydrogen on the H_2-preactivated ruthenium surface has decreased after some conversion of linoleic acid, the dehydrogenation mechanism starts to play a role. At the same time, systematic deviations were visible for both models, therefore calling for incorporation of catalyst deactivation in the kinetic modeling. Catalyst deactivation steps of four different orders were introduced to the mechanisms and mathematically modeled. Model C(2) describing the isomerization of linoleic acid via the dehydrogenation mechanism with second order catalyst deactivation involved, showed lowest SRS and estimated relative standard error of the parameters as well as the highest R^2 of all investigated models and a more or less perfect data fitting. This can be an indication that the mechanistic data of model C(2) is most consistent with observed kinetic regularities. Moreover, parity plots gave better linearly collected data points for model C(2) than for other models and sensitivity analyses showed rather clear minima of the objective function versus the parameters of this model.

Acknowledgments

This work is part of the activities at the Åbo Akademi Process Chemistry Centre within the Finnish Centre of Excellence Programme (2000–2005) by the Academy of Finland. Financial support from the Raisio Group Research Foundation is gratefully acknowledged.

References

[1] A. Bernas, N. Kumar, P. Mäki-Arvela, E. Laine, B. Holmbom, T. Salmi, D.Yu. Murzin, Conjugation of linoleic acid over a hydrogen preactivated heterogeneous catalyst, Chem. Commun. 10 (2002) 1142–1143.
[2] A. Bernas, P. Laukkanen, N. Kumar, P. Mäki-Arvela, J. Väyrynen, E. Laine, B. Holmbom, T. Salmi, D.Yu. Murzin, A new heterogeneously catalytic pathway for isomerization of linoleic acid over Ru/C and Ni/H-MCM-41 catalysts, J. Catal. 210 (2002) 354–366.
[3] A. Bernas, N. Kumar, P. Mäki-Arvela, N.V. Kul'kova, B. Holmbom, T. Salmi, D.Yu. Murzin, Isomerization of linoleic acid over supported metal catalysts, Appl. Catal. A: Gen. 245 (2003) 257–275.
[4] A. Bernas, P. Mäki-Arvela, N. Kumar, B. Holmbom, T. Salmi, D.Yu. Murzin, Heterogeneously catalytic isomerization of linoleic acid over supported ruthenium catalysts for production of anticarcinogenic food constituents, Ind. Eng. Chem. Res. 42 (2003) 718–727.
[5] A. Bernas, D.Yu. Murzin, Influence of hydrogen preactivation on the linoleic acid isomerization properties of supported ruthenium catalysts, React. Kinet. Catal. Lett. 78 (2003) 3–10.
[6] A. Bernas, N. Kumar, P. Mäki-Arvela, B. Holmbom, T. Salmi, D.Yu. Murzin, Heterogeneous catalytic production of conjugated linoleic acid, Org. Proc. Res. Dev. 8 (2004) 341–352.
[7] A. Bernas, D.Yu. Murzin, Linoleic acid isomerization on Ru/Al2O3 catalyst. 1. Conjugation and hydrogenation, Chem. Eng. J. 115 (2005) 13–22.
[8] H. Pines, The Chemistry of Catalytic Hydrocarbon Conversions, Academic Press, New York, 1981.
[9] N.C. Ramani, D.L. Sullivan, J.G. Ekerdt, Isomerization of 1-butene over silica-supported Mo(VI), W(VI), and Cr(VI), J. Catal. 173 (1998) 105–114.
[10] M.I. Temkin, The kinetics of some industrial heterogeneous catalytic reactions, Adv. Catal. 28 (1979) 173.
[11] J. Horiuti, Res. Inst. Catal. Hokkaido Univ. 5 (1957) 1.
[12] H. Haario, Modest User's Guide, Helsinki, 2001.
[13] O. Levenspiel, Chemical Reaction Engineering, third ed., Wiley, New York, 1999.
[14] B. Butt, E. Petersen, Activation, Deactivation, and Poisoning of Catalysts, Academic Press, London, 1988.